

THE REPUBLIC OF TUNISIA

MINISTRY OF AGRICULTURE

The Republic Of Tunisia
Preparatory Survey on Integrated Basin Management
and Flood Control Project for Mejerda River:
Climate Change Impact Analysis

FINAL REPORT

May 2013

JAPAN INTERNATIONAL COOPERATION AGENCY

THE UNIVERSITY OF TOKYO

GE
JR
13 - 134

THE REPUBLIC OF TUNISIA

MINISTRY OF AGRICULTURE

The Republic Of Tunisia
Preparatory Survey on Integrated Basin Management
and Flood Control Project for Mejerda River:
Climate Change Impact Analysis

FINAL REPORT

May 2013

JAPAN INTERNATIONAL COOPERATION AGENCY

THE UNIVERSITY OF TOKYO

Tunisian Republic

A Consideration of Climate Change Based on Mejerda Integrated Watershed Management and Flood

Study Survey Measures :

Mejerda Basin Climate Change Impact Assessment flood event riverflow development plan

Contents

Contents	1
List of Abbreviations	2
I Overview	4
(1) Background and objectives of this report	4
(2) Study Area	5
(3) Strategic Approaches	7
II Study Implementation	9
(1) Estimation of “design rainfall”, “design flood discharge before regulation” and “design flood discharge after regulation”	9
1 Design Rainfall and Design Flood Discharge before Regulation	9
1) Steps for the creation of design rainfall	10
2) Design Flood Discharge before Regulation	27
2 Design Flood Discharge after Regulation	35
1) Introduction of the Sidi Salem Dam Operation	35
2) Design Flood Discharge after the Sidi Salem Dam Operation	35
(2) Climate Change Impact Assessment of the Mejerda River Basin	37
1 Selection of the Emission Scenario	37
2 GCM Selection	38
3 Bias Correction of the Rainfall from the Selected GCMs	41
4 Assessment of Changes in Rainfall	48
5 Assessment of Changes in the Design Floods	51
(3) Optimizing Dam Operation	54
1 Hydrological Model	55
2 Global Optimization System	55
3 Rolling Horizon Approach	56
4 ISOS Procedure	57
5 ISOS Demonstration	57
III Conclusions and Recommendations	61
References	62
Appendix	63

Abbreviations

Abbreviation	English	French	Japanese
AfWCCI	GEOSS African Water Cycle Coordination Initiative	Initiative Africaine de la Coordination du Cycle de l'Eau	アフリカ水循環調整イニシアチブ
AIEM	Advanced Integral Equation Model	Modèle Avancé d'Equation Intégrale	表面散乱モデル
AMSR-E	Advanced Microwave Scanning Radiometer for EOS	Radiomètre Avancé à Balayage en Hyperfréquence	改良型高性能マイクロ波放射計
BATS	Biosphere-Atmosphere Transfer Scheme	Processus d'Echange entre la Biosphère et l'Atmosphère	陸面過程モデル
CMIP3	The 3rd phase of Coupled Model Intercomparison Project	La 3 ^e phase du Projet d'Inter-comparaison de Modèles Couplés	第3次モデル相互比較プロジェクト
C/P	Counterpart	Homologue	カウンターパート
DB	Database	Base de données	データベース
DEM	Digital Elevation Model	Modèle Numérique d'Altitude	数値標高モデル
DHM	Distributed Hydrological Model	Modèle Hydrologique Distribué	分布型水循環モデル
DMRT	Dense Medium Radiative Transfer	Modèle de Transfert Radiatif de Matériau Dense	放射伝達モデル
FAO	Food and Agriculture Organization of the United Nations	Organisation des Nations Unies pour l'Alimentation et l'Agriculture	国際連合食糧農業機関
FPAR	Fraction of Photosynthetic Active Radiation	Fraction de Rayonnement de Photosynthèse	光合成有効放射吸収率
F/R	Final Report	Rapport Final	ファイナル・レポート
GBHM	Geomorphology-Based Hydrological Model	Modèle Hydrologique à base de géomorphologie	分布型流出モデル
GCM	General Circulation Model	Modèle de la Circulation Générale	大気循環モデル
GEO	Group on Earth Observations	Groupe sur l'Observation de la Terre	地球観測作業部会
GEOSS	Global Earth Observation System of Systems	Réseau Mondial des Systèmes d'Observation de la Terre	全球地球観測システム
GOJ	Government of Japan	Gouvernement du Japon	日本国政府
GPS	Global Positioning System	Système de Positionnement Global (GPS)	全球測位システム
GSMaP	Global Satellite Mapping of Precipitation	Global Satellite Mapping of Precipitation	全球降水マップ
IC/R	Inception Report	Rapport de Commencement	インセプション・レポート
IPCC	Intergovernmental Panel on Climate Change	Groupe Intergouvernemental sur l'Evolution du Climat (GIEC)	気候変動に関する政府間パネル
IT/R	Interim Report	Rapport Intérimaire	インテリム・レポート
JCC	Joint Coordinating Committee	Comité de Coordination Conjoint	合同調整委員会
JICA	Japan International Cooperation Agency	Agence Japonaise de Coopération Internationale	国際協力機構
LAI	Leaf Area Index	Indice de Surface Foliaire	葉面積指数

LDAS-UT	Land Data Assimilation System by Coupling AMSR-E and SiB2	Système d'assimilation des données à la surface des terres émergées et Biosphère Simple 2	陸面データ同化
LSM	Land Surface Model	Modèle de la Surface de Terre	地表面モデル
M/M	Men Month	Homme Mois	人/月
NCDC	National Climatic Data Center	Centre National de Données Climatologiques	アメリカ国立気候データセンター
NOAA	National Oceanic and Atmospheric Administration	Administration Nationale Océanique et Atmosphérique	米国海洋大気庁
PDM	Project Design Matrix	Matrice de Conception du Projet	プロジェクト・デザイン・マトリックス
PO	Plan of Operation	Plan d'Exécution	実行計画
P/R	Progress Report	Rapport d'Avancement	プログレス・レポート
R/D	Record of Discussions	Procès-Verbaux	協議議事録
RMSE	Root Mean Squared Error	Erreur Quadratique Moyenne	2乗平均平方根誤差
RTM	Radiative Transfer Model	Modèle de Transfert Radiative	放射伝達モデル
SiB2	Simple Biosphere 2	Biosphère Simple 2	単純植生モデル2
SWI	Soil Wetness Index	Indice d'Humidité de Sol	土壌湿潤指数
USGS	United States Geological Survey	Commission Géologique des Etats-Unis	アメリカ地質調査所
WEB-DHM	Water and Energy Budget based Distributed Hydrological Model	Modèle Hydrologique Distribué, basé sur le budget d'eau et d'énergie	分布型水循環モデル
WMO	World Meteorological Organization	Organisation Météorologique Mondiale	世界気象機関
WRF	Weather Research and Forecasting. Model	Modèle Recherche Et Prévision Météo	次世代メソスケール数値天気予報モデルシステム
WSP	Water Security Plan	Plan de Sécurité de l'Eau	水の安全保障計画

I. Overview

(1) Background and objectives of this report

Mean annual rainfall over the Republic of Tunisia is 500 mm, and half of its area is within a semi-arid region. In the northern part of the country, including the Mejerda River Basin, there is large-scale heavy rainfall every several years during the rainy season, which continues from September to March. River flow increases suddenly and floods surrounding areas. Such heavy rainfall events occur more frequently especially in recent years. In 2000, 2003, 2004, 2005, 2009, and 2012, they have experienced large-scale flooding and inundation damage caused by heavy rainfall in the lower Mejerda basin. Among these events, the flooding of January 2003 resulted in 10 deaths and 27,000 evacuees. In addition, the inundation persisted for over a month, causing social and economic losses and affecting crops, housing, and transportation. Most recently, in February 2012, heavy rainfall in northwest Tunisia caused flooding in various parts of the Mejerda basin, creating enormous damage and a death toll of six. Such large-scale floods have associated with economic and social losses, such as economic stagnation and increase in disaster-related poverty, plus material losses on infrastructure and housing. Therefore, the large-scale disaster could be one of the important risk factors for this country to implement sustainable development.

The national government has implemented countermeasures against flooding. In the 11th Five-Year Socio-economic Development Plan (2007 to 2011), a strategy of reducing flood damage in urban areas was adopted and urban flooding countermeasures were planned, such as rainfall-drainage development projects and clearing of existing drainage systems. It is expected that such projects will have a synergetic effect with urban development and traffic planning.

In response to a request from the Government of The Republic of Tunisia, the Japan International Cooperation Agency (JICA) conducted a study on "The Study on Integrated Basin Management Focused on Flood Control in Mejerda River"(referred to hereafter as "Master Plan Study") for twenty-six months from 2006 to 2008, for the purpose of reduction of large-scale flooding and inundation damage in Mejerda River. The Master Plan Study developed a master plan for integrated river basin management which emphasizes flood control by combining structural measures including construction of river dike and retarding reservoir and non-structural ones including flood forecasting and warning, evacuation and flood fighting, organizational capacity development, flood plain regulation/management. In 2009, the government of Tunisia requested the Japanese government to do a feasibility study on this plan. Based on that request, the "Preparatory Survey on Integrated Basin Management and Flood Control Project for Mejerda in the Republic of Tunisia" (referred to hereinafter as "Preparatory Survey") was conducted from September 2010 to May 2012. The Preparatory Survey collected basic information and examined

fundamental countermeasures by targeting the most downstream area referred as “D2 Zone”.

To complement the Preparatory Survey and to develop more detailed implementation plan, the "Preparatory Survey on Integrated Basin Management and Flood Control Project for Mejerda River: Development of Flood Prevention Measures" (hereinafter referred to as "Preparatory Survey2") started in July 2012. However, Mejerda River locates in semi-arid region and is affected by heavy rainfall events so often recently due to disturbances in Mediterranean Sea. The Intergovernmental Panel on Climate Change (IPCC) 4th Assessment Report points that drought is likely to occur more frequently in North Africa. Considering the climatologically particularity of Mejerda River, sophisticated flood simulation and climate change impact assessment were implemented as a complementary survey to Preparatory Survey2 (hereinafter referred to as "Climate Change Impact Study").

This is the final report of Climate Change Impact Study, including the following three tasks:

- (1) To determine design rainfall, design flood discharge before regulation and design flood discharge after regulation
- (2) Climate change impact assessment
- (3) Optimization dam operation

The result of task (1) was used as a precondition to the Preparatory Survey2. The task (2) and (3) contributes to the direction of the future management of Mejerda River.

The overall structure of the Climate Change Impact Study is illustrated in **Figure I-(1)-1**.

(2) Surveyed Area

The target region is the lower basin of the Mejerda River in the Republic of Tunisia (governorates of Ariana, Manouba, and Bizerte), as shown in **Figure I-(1)-2** and **Figure I-(1)-3**. However, one of the targeted dams/reservoirs for examination of optimized operation of water-use facilities is the Sidi Salem Dam, in the middle basin of the Mejerda River.

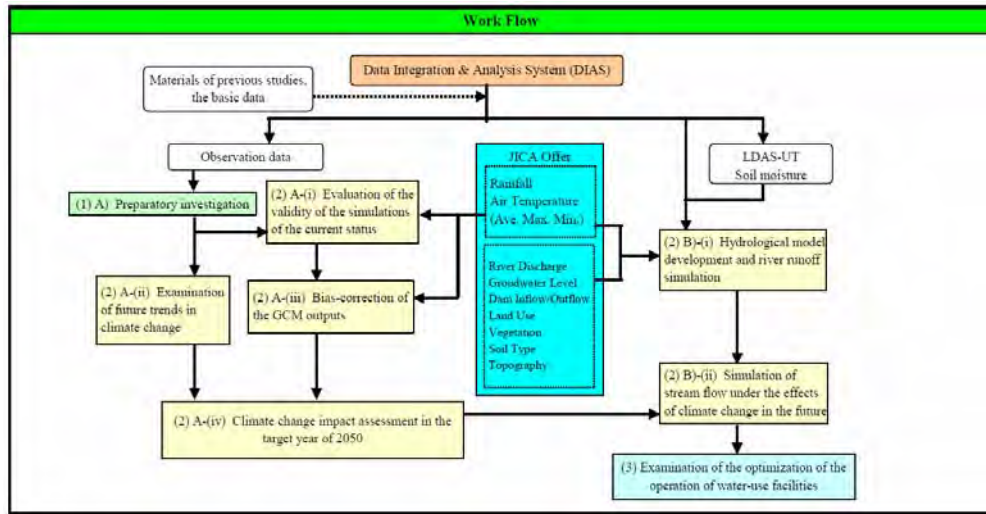


Figure I-(1)-1 Workflow of “Preparatory Survey on Integrated Basin Management and Flood Control Project for Mejerda River: Climate Change Impact Analysis”



Figure I-(1)-2 Location Map of the Study Area

Reference : THE STUDY ON INTEGRATED BASIN MANAGEMENT FOCUSED ON FLOOD CONTROL IN MEJERDA RIVER IN THE REPUBLIC OF TUNISIA: FINAL REPORT VOLUME-I EXECUTIVE SUMMARY JANUARY 2009

<http://libopac.jica.go.jp/images/report/P0000245729.html>

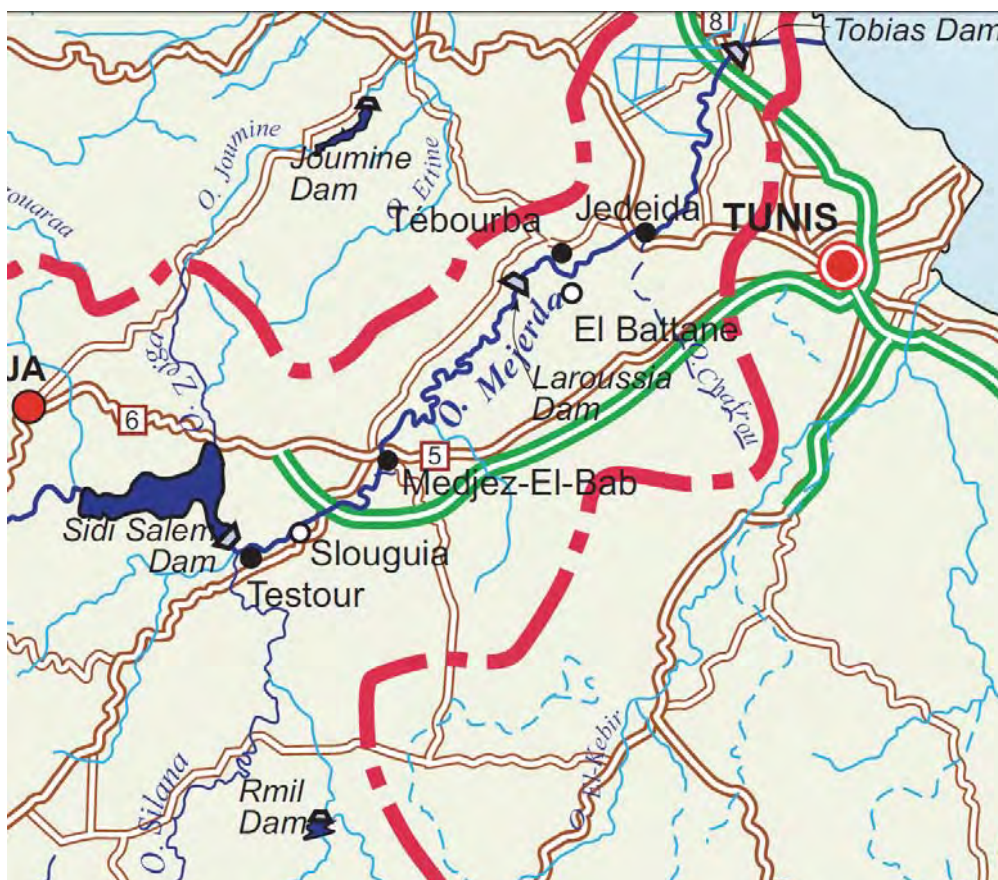


Figure I-(1)-3 Enlarged Map of the DownStream of the Mejerda

(3) Strategic Approaches

1) *Estimation of the design flood discharge in accordance with “design rainfall”, “design flood discharge before regulation” and “design flood discharge after regulation”*

To estimate “design rainfall” and “design flood discharge before regulation”, this report takes account of distribution characteristics of duration and temporal and spatial variations of rainfall in addition to rainfall probability. To simulate flood discharge of the Mejerda River, this report considers long-term continuous simulation capability of the river flow ranging from low to high level and the spatial distribution of soil moisture, which is closely related with a flood initial condition and its peak value. Taking account of the importance of spatial distributions of topography, soil type, vegetation and meteorological conditions, a distributed hydrological model which can express the river discharge and soilmoisture without any tuning after calibration should be used for this study. The Sidi Salem Dam operation is considered for estimating “design flood discharge after regulation” of the lower basin of the Mejerda River.

2) *Evaluating future climate change impact assessment*

To estimate climate change impact assessment, the General Circulation Model (hereinafter referred to GCM) is generally applicable. However, GCM cannot avoid uncertainty since there still have some unpredictable aspect in the physical and biochemical processes, and GCM has a large bias particularly in estimating rainfalls. Therefore, no quantitative assessment by one single GCM would be so appropriate. It is necessary to use multiple GCMs that can demonstrate meteorological characteristics in the target area, to examine the similarity of the obtained results, and to consider the range of assumption.

As the target spatio-scale for analyzing water cycle is generally smaller than a gridded size of GCM, a spatial downscaling scheme is important. While a bias correction by in-situ measurements is vital for a quantitative analysis. Some mechanical method such as a meso-scale non-hydrostatic model is widely used for a spatial downscaling, but their calculation cost is relatively high. Our target area has many rainfall observation stations, and long-termed data is available. In this study, we tried to express a spatial distribution by interpolating and extrapolating a bias-corrected model output data corresponding to each rainfall observation stations.

3) Optimum Operation

Optimum operation in water facilities is under review. Given that the length of river flow is quite long in the Mejerda River Basin, with considering the flood travel time as a lead time for flood prediction, this study performs an inflow forecasting in the Sidi Salem Dam, and develops an optimization method of evaluation function for contributing to a flood disaster mitigation.

II. Study Implementation

(1) Estimation of “design rainfall”, “design flood discharge before regulation” and “design flood discharge after regulation”

This study estimates “design rainfall”, “design flood discharge before regulation” and “design flood discharge after regulation” according to the following workflow chart:

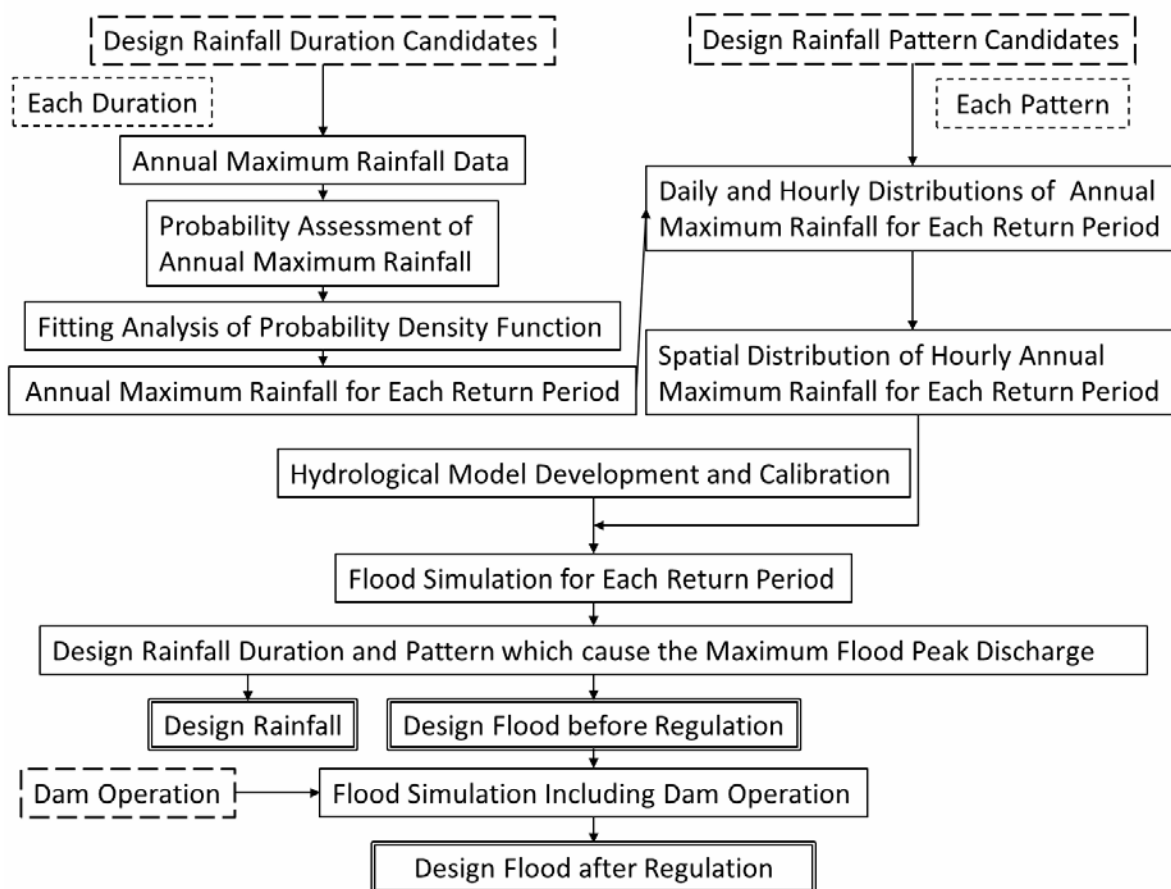


Figure II-(1)-1 Work Flow of this Study

1. Design Rainfall and Design Flood Discharge before Regulation

The preparatory survey was done on a selected past flood events occurred in the Mejerda River Basin . For the identification of extreme events, the maximum daily rainfall and the number of days of continuous rain for each event were calculated by the two thresholds from two different rainfall quantities respectively. Based on the rainfall duration in days, a probability

evaluation of the corresponding average rainfall values was performed and a precipitation map was calculated. This precipitation map and past flood cases were correlated with average daily precipitation (assigned for each day); these daily values were then decomposed into hourly accumulations for the purpose of performing flood runoff simulation. After creating the spatial distribution of daily precipitation measurements during the past flood events, a gridded dataset of hourly precipitation data was established.

The geological characteristics, soil properties, land use characteristics, and additional observed data of the Mejerda River Basin watershed, were used to calibrate WEB-DHM, a distributed runoff model incorporating water cycle simulation and capable of representing hydrological characteristics of the watershed. After confirming the reproducibility of flood runoff characteristics for these past scenarios, the design rainfall scenarios were evaluated to obtain the corresponding river flood discharge. For each rainfall duration event measured in days, the maximum and expected flood discharge corresponding to spatial and temporal distribution of rainfall was determined.

1) Steps for the creation of design rainfall

a. Watershed classification and data extraction

Figure II-(1)-2 shows the distribution of rainfall observation sites available for this study and the identification of sub-basins following the major tributaries of the Mejerda . Rainfall data could not be obtained for the sub-basins located in the upstream portion of the Mejerda (sub-basin 9 and portions of 6) which is located in Algerian territory. In other areas of the watershed there are a sufficient number of daily rainfall measurement stations for analysis. Using observations from these points it is possible to determine the characteristics of the spatio-temporal distribution of precipitation.

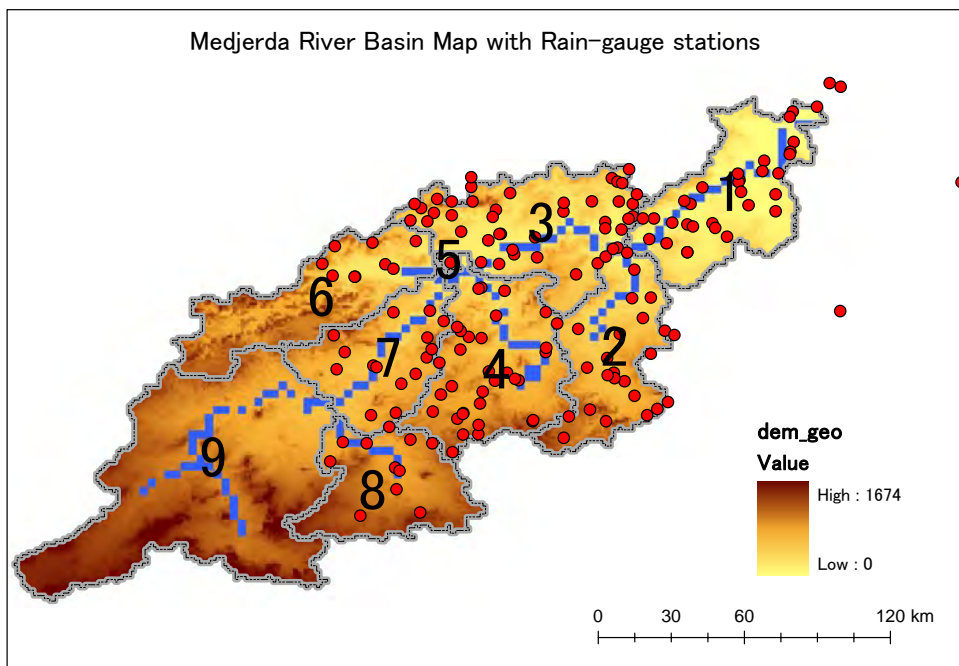


Figure II-(1)-2 Mejerda Observation Points and Sub-basin Identification

b. Extraction of continuous rain events and annual maximum precipitation data

For calculating the number of continuous rain days, based on the past flood data (Mar. 1973, May 2000, Jan. 2003, Dec. 2003), two methods of examination were considered:

1. Number of contiguous days with over 20mm/day (**Figure II-(1)-3**, red) rainfall.
2. Number of contiguous days with over 10mm/day (**Figure II-(1)-3**, pink) rainfall.

Considering the Differences in sub-basins at the movement of rainy area, the window for averaging rainfall data indicated four days in case 1 (20mm/day) and five days in case 2 (10mm/day) .

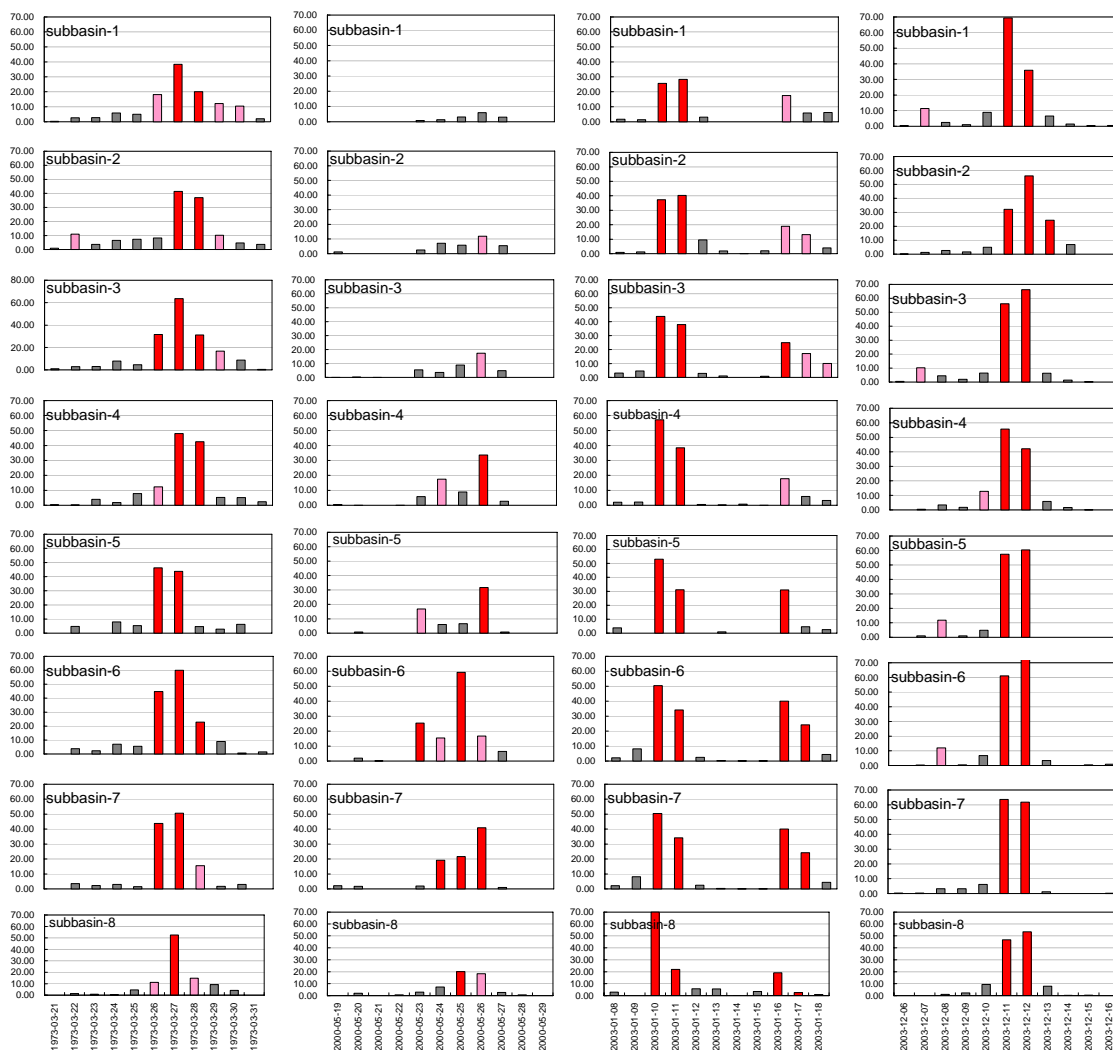


Figure II-(1)-3 Height graph for each sub-basin during previous four flood periods (red: over 20mm/day continuous rainfall, pink: between 10mm/day and 20mm/day continuous rainfall)

Table II-(1)-1 shows collected data between 1950 and 2007 for annual maximum daily, 4-day and 5-day rainfall.

Table II-(1)-1 1950~2007 annual maximum daily, 4-day and 5-day rainfall

year	daily rainfall[mm]	4-day rainfall[mm]	5-day rainfall[mm]
1950	28.73	42.97	52.75
1951	23.53	56.14	66.31
1952	36.16	82.43	89.58
1953	44.70	77.57	77.79
1954	20.89	47.24	52.01
1955	25.94	52.09	54.41
1956	31.70	67.17	70.45
1957	43.04	78.11	80.77
1958	28.65	48.60	54.77
1959	30.91	65.86	68.86
1960	14.91	26.12	26.30
1961	26.18	48.52	48.55
1962	33.92	78.14	85.82
1963	22.85	48.32	51.25
1964	46.59	76.36	76.62
1965	12.29	35.59	40.94
1966	23.51	56.43	56.65
1967	12.77	36.05	38.85
1968	19.40	41.16	43.68
1969	40.49	82.83	100.18
1970	27.44	51.80	51.92
1971	32.58	61.63	62.46
1972	30.66	52.38	55.62
1973	50.16	111.97	118.64
1974	23.70	59.18	63.01
1975	34.98	75.66	77.32
1976	27.94	73.75	75.85
1977	16.96	40.34	42.70
1978	17.18	41.33	50.54
1979	37.09	77.08	77.92
1980	24.46	46.89	47.35
1981	10.55	50.65	52.58
1982	25.16	52.66	59.18
1983	20.08	44.01	44.43
1984	38.84	98.02	100.38
1985	13.74	97.34	104.47
1986	17.18	39.91	42.86
1987	20.94	40.97	41.84
1988	25.64	43.93	46.41
1989	15.28	38.84	40.13
1990	32.22	67.36	81.41
1991	26.22	46.13	54.58
1992	34.84	63.26	65.54
1993	10.88	25.44	31.28
1994	17.44	45.78	51.92
1995	13.39	35.09	41.02
1996	26.58	66.93	70.17
1997	20.30	45.03	47.59
1998	28.55	45.39	47.51
1999	21.24	42.77	49.64
2000	21.27	49.47	62.63
2001	22.33	35.14	35.56
2002	22.09	45.86	49.93
2003	55.02	126.41	128.40
2004	43.05	72.08	76.72
2005	35.98	65.04	69.11
2006	33.69	60.36	68.52
2007	26.12	76.65	86.48

c. Selection of probability density function for the probability estimation of basin average annual maximum precipitation

In order to interpolate the expected rainfall in each analysis interval, eleven potential probability density functions (PDF) were evaluated with respect to annual maximum 4-day and 5-day rainfall as outlined in **Table II-(1)-1**. These PDFs are as follows; the exponential distribution function (Exp), the Gumbel distribution (Gumbel), the square-root exponential distribution of maximum likelihood (SqrtEto), the generalized extreme value distribution (Gev), the Pearson logarithmic type III distribution (law-logarithmic space) (logP3), the Iwai law (Iwai), the Ishihara Takase law (IshiTaka), the log-normal 3-parameter Kwon tile distribution (LN3Q), the log-normal 3-parameter distribution (Slade II)(LN3PM), the log-normal 2-parameter distribution (Slade I, L factor)(LN2LM), and the log-normal 2-parameter distribution (Slade I, factor)(LN2PM). The results are outlined in Table II-(1)-2 and **Table II-(1)-3**. An analysis of fit was done for each probability density function as shown in **Figure II-(1)-4** and **Figure II-(1)-5**.

The standard least squares criteria (SLSC) of the fitness evaluation were found, and the results were evaluated in accordance with the jackknife method for stability assessment. The square-root exponential of maximum value distribution (SqrtEto) was found to have a very low estimation error based on the jackknife method and in comparison with other distributions. The SLSC for this distribution was as low as 0.03. This analysis was done over the range of collected data during the period of 1950-2007, while "Preparatory Survey"(JICA, 2009) conducted the same study for the years of 1968-2005. The two studies showed the similar result when application of the distribution SqrtEto. Therefore it was decided to adopt square-root exponential of maximum value distribution (SqrtEto) for its higher stability.

Table II-(1)-2 Evaluation of Max. Annual 4-day Probability of Precipitation

Exponential distrib.											
SLSC(99%)	X-COR(99%)	P-COR(99%)	Exp	Log likelihood	pAIC	SLSC(50%)	X-COR(50%)	P-COR(50%)			
0.038	0.983	0.947	-237.7	479.4	0.053	0.984	0.977				
Return Period	400	200	150	100	80	50	30	20	10	5	3
Probability Rainfall	165.6	153.2	146.8	137.8	132.9	122.5	111.1	102.2	86.8	71.4	60.1
Jackknife Estimate	166.5	153.2	146.8	137.8	132.9	122.5	111.1	102.2	86.8	71.4	60.1
Jackknife Est. Err.	14.5	13.2	12.4	11.4	10.8	9.6	8.3	7.5	6.6	5.6	4.6
Gumbel distrib.											
SLSC(99%)	X-COR(99%)	P-COR(99%)	Gumbel	Log likelihood	pAIC	SLSC(50%)	X-COR(50%)	P-COR(50%)			
0.026	0.992	0.992	-250.6	505.1	0.045	0.988	0.979				
Return Period	400	200	150	100	80	50	30	20	10	5	3
Probability Rainfall	144.5	133.4	128.8	122.2	118.7	111.1	102.8	96.2	84.7	72.7	63.1
Jackknife Estimate	144.5	133.4	128.8	122.2	118.7	111.1	102.9	96.2	84.7	72.7	63.1
Jackknife Est. Err.	12.1	10.9	10.3	9.6	9.2	8.3	7.4	6.6	5.3	4.1	3.1
Sqrt-exp Max. value											
SLSC(99%)	X-COR(99%)	P-COR(99%)	SqrtExp	Log likelihood	pAIC	SLSC(50%)	X-COR(50%)	P-COR(50%)			
0.031	0.991	0.994	-250.8	505.6	0.057	0.985	0.979				
Return Period	400	200	150	100	80	50	30	20	10	5	3
Probability Rainfall	182.8	183.1	155.3	144.5	138.7	126.8	114.4	104.9	89.3	74.3	63.2
Jackknife Estimate	182.6	183	155.1	144.4	138.6	126.7	114.3	104.8	89.2	74.1	63.1
Jackknife Est. Err.	3.8	3.6	3.4	3.4	3.4	3.2	3.1	3	2.8	2.6	2.4
Generalized extreme value											
SLSC(99%)	X-COR(99%)	P-COR(99%)	Gev	Log likelihood	pAIC	SLSC(50%)	X-COR(50%)	P-COR(50%)			
0.024	0.993	0.993	-250.3	506.7	0.042	0.986	0.976				
Return Period	400	200	150	100	80	50	30	20	10	5	3
Probability Rainfall	158.1	143.1	137	127	124	114.9	106	97.4	84.6	71.9	62.2
Jackknife Estimate	155.1	141.8	136	128.1	123.8	114.8	105.2	97.6	84.8	72	62.2
Jackknife Est. Err.	29.8	22.4	19.8	16.4	14.7	11.7	9	7.3	5.3	4.1	3.4
Pearson logarithmic type III											
SLSC(99%)	X-COR(99%)	P-COR(99%)	LogP3	Log likelihood	pAIC	SLSC(50%)	X-COR(50%)	P-COR(50%)			
0.028	0.993	0.993	-250.3	506.7	0.047	0.993	0.993				
Return Period	400	200	150	100	80	50	30	20	10	5	3
Probability Rainfall	151.9	138.5	133.1	125.6	121.5	113	103.9	96.8	84.7	72.3	62.7
Jackknife Estimate	149	136.7	131.7	124.6	120.7	112.6	103.8	96.8	84.8	72.4	62.7
Jackknife Est. Err.	24.3	19.1	17.2	14.7	13.5	11.1	8.9	7.4	5.4	4	3.2
Iwai law											
SLSC(99%)	X-COR(99%)	P-COR(99%)	Iwai	Log likelihood	pAIC	SLSC(50%)	X-COR(50%)	P-COR(50%)			
0.029	0.992	0.993	-250.4	506.7	0.05	0.988	0.979				
Return Period	400	200	150	100	80	50	30	20	10	5	3
Probability Rainfall	144.7	133.3	128.6	122	118.3	110.7	102.5	96.9	84.5	72.5	63
Jackknife Estimate	162.6	138.5	134.2	126.7	122.7	114.1	104.9	97.7	85.2	72.4	62.4
Jackknife Est. Err.	24.5	20.1	18.3	16	14.8	12.4	10	8.3	5.8	3.8	2.8
Ishihara Takase											
SLSC(99%)	X-COR(99%)	P-COR(99%)	IshiTaka	Log likelihood	pAIC	SLSC(50%)	X-COR(50%)	P-COR(50%)			
0.03	0.993	0.993	-250.3	506.7	0.049	0.988	0.977				
Return Period	400	200	150	100	80	50	30	20	10	5	3
Probability Rainfall	148.1	138.2	131.1	124	120.1	112	103.2	96.3	84.4	72.2	62.6
Jackknife Estimate	147.5	135.7	130.8	124	120.2	112.4	103.8	96.9	85	72.6	62.8
Jackknife Est. Err.	21.1	17	15.5	13.5	12.5	10.4	8.5	7.2	5.4	4.1	3.4
log-normal 3 param Kwon til LN3Q											
SLSC(99%)	X-COR(99%)	P-COR(99%)	LN3Q	Log likelihood	pAIC	SLSC(50%)	X-COR(50%)	P-COR(50%)			
0.03	0.993	0.993	-250.4	506.7	0.048	0.988	0.978				
Return Period	400	200	150	100	80	50	30	20	10	5	3
Probability Rainfall	151.1	138.1	132.8	125.5	121.4	113.1	104.1	97	84.8	72.3	62.6
Jackknife Estimate	157.7	143.4	137.6	129.6	125.2	116.1	106.3	98.7	85.7	72.6	62.4
Jackknife Est. Err.	20.7	17.3	15.9	14.1	13.1	11.2	9.3	7.8	5.7	3.9	2.9
Log-normal 3 param LN3PM											
SLSC(99%)	X-COR(99%)	P-COR(99%)	LN3PM	Log likelihood	pAIC	SLSC(50%)	X-COR(50%)	P-COR(50%)			
0.029	0.993	0.993	-250.3	506.7	0.049	0.988	0.978				
Return Period	400	200	150	100	80	50	30	20	10	5	3
Probability Rainfall	147.5	135.4	130.4	123.4	119.6	111.7	103.1	96.2	84.5	72.3	62.7
Jackknife Estimate	145.2	134	129.4	122.9	119.3	111.7	103.4	96.8	85.1	72.9	63.1
Jackknife Est. Err.	20.6	16.7	15.3	13.3	12.3	10.4	8.5	7.2	5.4	4.1	3.4
Log-normal 2 param L LN2LM											
SLSC(99%)	X-COR(99%)	P-COR(99%)	LN2LM	Log likelihood	pAIC	SLSC(50%)	X-COR(50%)	P-COR(50%)			
0.029	0.991	0.992	-250.5	505	0.053	0.988	0.979				
Return Period	400	200	150	100	80	50	30	20	10	5	3
Probability Rainfall	140.7	130.1	125.8	119.7	116.3	109.2	101.4	95.2	84.3	72.7	63.3
Jackknife Estimate	139.9	129.5	125.2	119.2	115.8	108.8	101.1	94.9	84.1	72.6	63.2
Jackknife Est. Err.	14.7	12.8	12	10.9	10.3	9.2	7.9	7	5.4	4	3
Log-normal 2 param F LN2PM											
SLSC(99%)	X-COR(99%)	P-COR(99%)	LN2PM	Log likelihood	pAIC	SLSC(50%)	X-COR(50%)	P-COR(50%)			
0.03	0.991	0.992	-250.5	505	0.054	0.988	0.979				
Return Period	400	200	150	100	80	50	30	20	10	5	3
Probability Rainfall	140.2	129.8	125.4	119.4	116	108.9	101.2	95	84.1	72.6	63.3
Jackknife Estimate	140	129.6	125.3	119.3	115.9	108.9	101.2	95	84.1	72.6	63.2
Jackknife Est. Err.	14.2	12.4	11.6	10.6	10	8.9	7.7	6.8	5.3	3.9	3

Table II-(1)-3 Evaluation of Max. Annual 5-day Probability of Precipitation

Exponential distrib. Exp									
SLSC(99%)	X-COR(99%)	P-COR(99%)	Log likelihood	pAIC	SLSC(50%)	X-COR(50%)	P-COR(50%)		
0.038	0.883	0.945	-240.4	484.8	0.052	0.99	0.884		
Return Period	400	200	150	100	80	50	30	20	10
Probability Rainfall	178.2	162.1	155.4	146	140.8	129.9	118	108.6	92.5
Jackknife Estimate	178.2	162.1	155.4	146	140.8	129.9	118	108.6	92.5
Jackknife Est. Err.	15.2	13.4	12.6	11.8	11	9.8	8.4	7.4	5.7
Gumbel distrib. Gumbel									
SLSC(99%)	X-COR(99%)	P-COR(99%)	Log likelihood	pAIC	SLSC(50%)	X-COR(50%)	P-COR(50%)		
0.02	0.995	0.995	-253.4	510.7	0.032	0.993	0.988		
Return Period	400	200	150	100	80	50	30	20	10
Probability Rainfall	152.9	141.3	138.5	129.9	125.9	117.9	109.3	102.3	90.3
Jackknife Estimate	152.9	141.3	138.5	129.9	125.9	117.9	109.3	102.3	90.3
Jackknife Est. Err.	12.3	11	10.5	9.7	9.3	8.4	7.5	6.7	5.4
Scri1 exp. Max. value SarrEto									
SLSC(99%)	X-COR(99%)	P-COR(99%)	Log likelihood	pAIC	SLSC(50%)	X-COR(50%)	P-COR(50%)		
0.028	0.993	0.996	-263.7	511.4	0.051	0.989	0.988		
Return Period	400	200	150	100	80	50	30	20	10
Probability Rainfall	189.7	169.7	161.7	150.7	144.8	132.7	120.1	110.3	94.4
Jackknife Estimate	189.7	169.7	161.7	150.7	144.8	132.7	119.9	110.2	94.2
Jackknife Est. Err.	4	3.8	3.7	3.8	3.5	3.4	3.2	3.1	2.9
Generalized extreme value Gev									
SLSC(99%)	X-COR(99%)	P-COR(99%)	Log likelihood	pAIC	SLSC(50%)	X-COR(50%)	P-COR(50%)		
0.019	0.995	0.996	-253.3	512.5	0.033	0.991	0.984		
Return Period	400	200	150	100	80	50	30	20	10
Probability Rainfall	164.3	149.4	143.4	135.1	130.5	121.1	111.2	103.4	90.2
Jackknife Estimate	161.8	148.1	142.5	134.5	130.2	121.1	111.3	103.6	90.4
Jackknife Est. Err.	27.9	21.2	18.7	15.7	14.2	11.4	8.9	7.3	5.4
Pearson logarithmic type II LogP3									
SLSC(99%)	X-COR(99%)	P-COR(99%)	Log likelihood	pAIC	SLSC(50%)	X-COR(50%)	P-COR(50%)		
0.022	0.996	0.995	-253.3	512.5	0.035	0.996	0.995		
Return Period	400	200	150	100	80	50	30	20	10
Probability Rainfall	157.3	144.1	138.8	131.4	127.3	118.8	109.7	102.5	90.2
Jackknife Estimate	154.5	142.4	137.4	130.4	126.5	118.4	109.5	102.5	90.3
Jackknife Est. Err.	23.3	18.4	16.8	14.2	13.1	10.8	9.7	7.3	5.4
Iwai law Iwai									
SLSC(99%)	X-COR(99%)	P-COR(99%)	Log likelihood	pAIC	SLSC(50%)	X-COR(50%)	P-COR(50%)		
0.025	0.996	0.996	-253.3	512.7	0.035	0.992	0.988		
Return Period	400	200	150	100	80	50	30	20	10
Probability Rainfall	161.1	147.4	141.8	134	129.7	120.8	111.3	103.8	90.8
Jackknife Estimate	170.2	154.7	148.3	139.6	134.8	124.9	114.3	106	92
Jackknife Est. Err.	23.7	19.4	17.7	15.5	14.4	12.1	9.8	8.2	5.9
Ishihara Takase IshiTakae									
SLSC(99%)	X-COR(99%)	P-COR(99%)	Log likelihood	pAIC	SLSC(50%)	X-COR(50%)	P-COR(50%)		
0.023	0.996	0.995	-253.3	512.5	0.038	0.992	0.988		
Return Period	400	200	150	100	80	50	30	20	10
Probability Rainfall	153.3	141.2	136.3	129.3	125.5	117.5	108.8	101.9	89.9
Jackknife Estimate	151.6	140.2	135.5	128.9	125.3	117.5	109.1	102.3	90.4
Jackknife Est. Err.	17.3	14.7	13.5	11.9	11.1	9.5	7.9	6.9	5.4
log-normal 3 param Kwon t LN3Q									
SLSC(99%)	X-COR(99%)	P-COR(99%)	Log likelihood	pAIC	SLSC(50%)	X-COR(50%)	P-COR(50%)		
0.023	0.996	0.995	-253.3	512.5	0.038	0.992	0.988		
Return Period	400	200	150	100	80	50	30	20	10
Probability Rainfall	153	141	136.1	129.1	125.4	117.4	108.7	101.8	89.9
Jackknife Estimate	143.1	133.6	129.6	123.9	120.7	114	106.5	100.4	89.6
Jackknife Est. Err.	18.5	15.1	13.8	12.2	11.3	9.6	8	6.9	5.3
Log-normal 3 param LN3PM									
SLSC(99%)	X-COR(99%)	P-COR(99%)	Log likelihood	pAIC	SLSC(50%)	X-COR(50%)	P-COR(50%)		
0.023	0.996	0.995	-253.3	512.5	0.038	0.993	0.988		
Return Period	400	200	150	100	80	50	30	20	10
Probability Rainfall	152.2	140.4	135.6	128.8	125	117.2	108.6	101.8	90
Jackknife Estimate	149.7	138.9	134.4	128	124.4	117	108.8	102.1	90.5
Jackknife Est. Err.	17.5	14.4	13.3	11.7	10.9	9.4	7.9	6.9	5.4
Log-normal 2 param L LN2LM									
SLSC(99%)	X-COR(99%)	P-COR(99%)	Log likelihood	pAIC	SLSC(50%)	X-COR(50%)	P-COR(50%)		
0.023	0.995	0.994	-253.4	510.8	0.04	0.993	0.987		
Return Period	400	200	150	100	80	50	30	20	10
Probability Rainfall	148.4	137.6	133.1	126.8	123.3	115.9	107.8	101.3	89.9
Jackknife Estimate	147.7	138.9	132.5	126.2	122.8	115.5	107.5	101.1	89.7
Jackknife Est. Err.	15	13.1	12.3	11.2	10.6	9.4	8.1	7.2	5.6
Log-normal 2 param F LN2PM									
SLSC(99%)	X-COR(99%)	P-COR(99%)	Log likelihood	pAIC	SLSC(50%)	X-COR(50%)	P-COR(50%)		
0.024	0.995	0.994	-253.4	510.8	0.041	0.993	0.987		
Return Period	400	200	150	100	80	50	30	20	10
Probability Rainfall	147.6	138.9	132.4	126.1	122.7	115.4	107.4	101	89.7
Jackknife Estimate	147.4	139.7	132.3	126.1	122.8	115.4	107.4	101	89.7
Jackknife Est. Err.	14.4	12.5	11.8	10.8	10.2	9	7.8	6.9	5.4

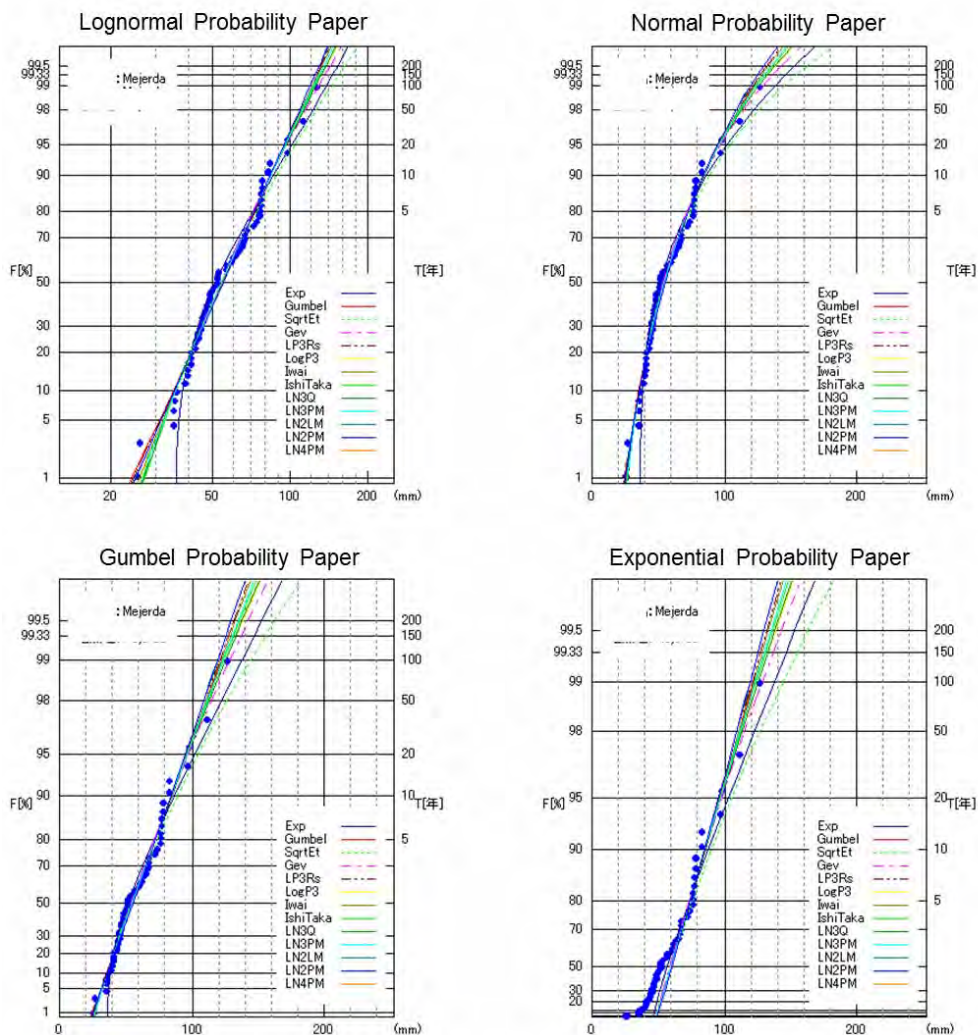


Figure II-(1)-4 4-day rainfall distribution regression

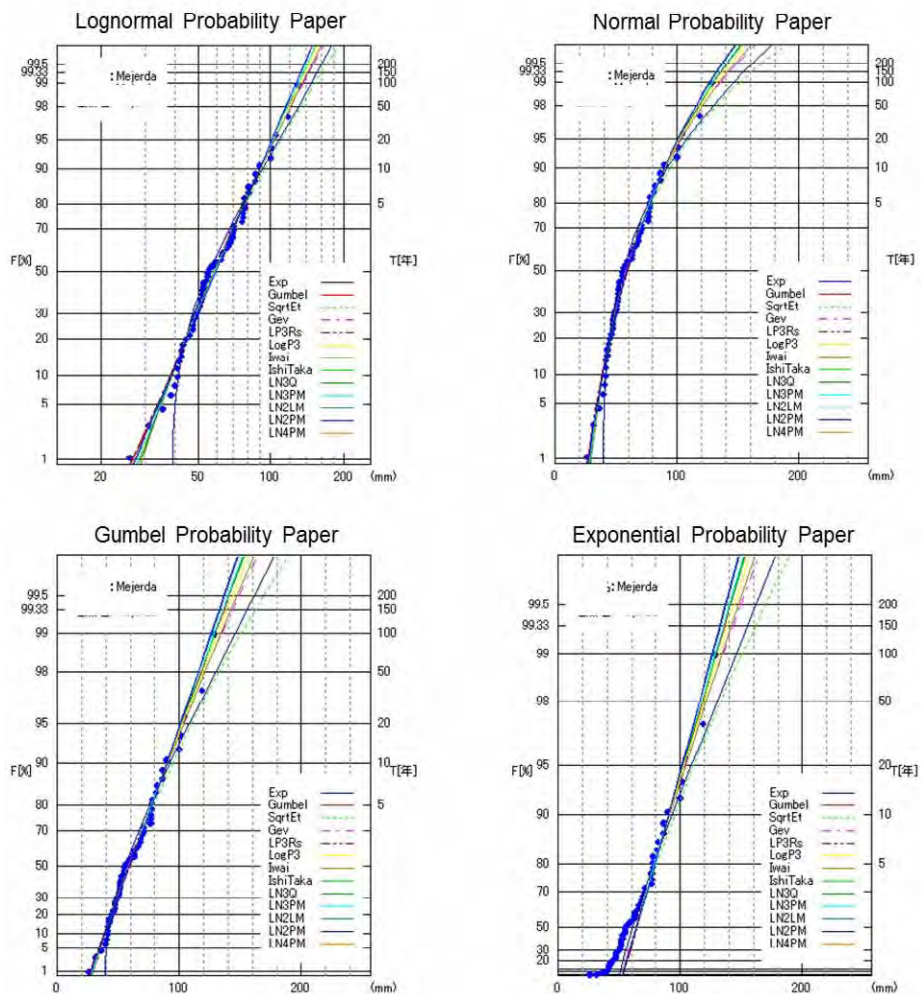


Figure II-(1)-5 5-day rainfall distribution regression

d. Calculation of daily and hourly distribution of precipitation probability data

Creating the daily rainfall data

The square root exponential distribution of maximum likelihood (SqrtEto) was estimated for 4-day and 5-day rainfall periods, with probability of precipitation for the past flood periods (Mar.1973, May 2000, Jan.2003, and Dec.2003). Based on the ratio of daily distribution to cumulative distribution, daily precipitation amounts were allocated with results as shown in **Table II-(1)-4**. For example, in the case of the Mar.1973 flood period, the total 5-day rainfall is 118.64mm. The daily breakdown was 22.36mm for Mar. 26, 50.16mm for Mar. 27, and 28.29mm for Mar. 28, and so on. Given the total rainfall period is for 4 days, each day ratio through Mar. 26 and Mar. 29 in the total rainfall (111.97mm) was evaluated as 0.20, 0.45, 0.26, 0.09 in series. Considering the 5-day accumulated rainfall between Mar. 26 and Mar. 30, the daily percentage of total rainfall is outlined in the table.

The 100-year precipitation probability over the 4-day period is 144.50mm, so the rainfall which is assumed to have fallen on Mar. 26, 0.20 of the 144.50mm total, is 28.86mm. In the same way other daily precipitation probabilities can be calculated by the corrected precipitation values.

Table II-(1)-4 Distribution of annual maximum rainfall for each day of the return period

Basin avg.	Rainfall			Probability of precipitation											
	daily	4-day	5-day	100 year		50 year		20 year		10 year		5 year		2 year	
				4-day	5-day	4-day	5-day	4-day	5-day	4-day	5-day	4-day	5-day	4-day	5-day
Accum. Val	118.64	1.00	1.00	144.50	150.70	126.80	132.70	104.90	110.30	89.30	94.40	74.30	78.90	53.90	57.90
1973/3/26	22.36	0.20	0.19	28.86	28.40	25.32	25.01	20.95	20.79	17.83	17.79	14.84	14.87	10.76	10.91
1973/3/27	50.16	0.45	0.42	64.73	63.71	56.80	56.10	46.99	46.63	40.00	39.91	33.28	33.36	24.15	24.48
1973/3/28	28.89	0.26	0.24	37.28	36.70	32.71	32.31	27.06	26.86	23.04	22.99	19.17	19.21	13.91	14.10
1973/3/29	10.56	0.09	0.09	13.63	13.42	11.96	11.82	9.90	9.82	8.42	8.41	7.01	7.03	5.08	5.16
1973/3/30	6.67		0.06	0.00	8.47	0.00	7.46	0.00	6.20	0.00	5.30	0.00	4.43	0.00	3.25
Accum. Val	48.34	1.00	1.00	144.50	150.70	126.80	132.70	104.90	110.30	89.30	94.40	74.30	78.90	53.90	57.90
2000/5/23	4.61	0.10	0.10	14.97	14.36	13.13	12.65	10.86	10.51	9.25	9.00	7.70	7.52	5.58	5.52
2000/5/24	8.50	0.19	0.18	27.61	26.50	24.23	23.33	20.04	19.39	17.06	16.60	14.20	13.87	10.30	10.18
2000/5/25	11.69	0.26	0.24	37.97	36.44	33.32	32.09	27.56	26.67	23.46	22.83	19.52	19.08	14.16	14.00
2000/5/26	19.69	0.44	0.41	63.96	61.38	56.12	54.05	46.43	44.93	39.53	38.45	32.89	32.14	23.86	23.58
2000/5/27	3.86		0.08	0.00	12.02	0.00	10.58	0.00	8.80	0.00	7.53	0.00	6.29	0.00	4.62
Accum. Val	89.79	1.00	1.00	144.50	150.70	126.80	132.70	104.90	110.30	89.30	94.40	74.30	78.90	53.90	57.90
2003/1/8	2.25		0.03	0.00	3.77	0.00	3.32	0.00	2.76	0.00	2.36	0.00	1.97	0.00	1.45
2003/1/9	2.34	0.03	0.03	3.86	3.92	3.38	3.45	2.80	2.87	2.38	2.46	1.98	2.05	1.44	1.51
2003/1/10	45.88	0.52	0.51	75.73	77.00	66.45	67.80	54.97	56.36	46.80	48.23	38.94	40.31	28.25	29.58
2003/1/11	35.80	0.41	0.40	59.09	60.08	51.85	52.90	42.89	43.97	36.52	37.63	30.38	31.46	22.04	23.08
2003/1/12	3.53	0.04	0.04	5.83	5.93	5.12	5.22	4.23	4.34	3.60	3.71	3.00	3.10	2.18	2.28
Accum. Val	128.40	1.00	1.00	144.50	150.70	126.80	132.70	104.90	110.30	89.30	94.40	74.30	78.90	53.90	57.90
2003/12/10	7.98	0.06	0.06	9.12	9.36	8.00	8.24	6.62	6.85	5.64	5.87	4.69	4.90	3.40	3.60
2003/12/11	54.92	0.43	0.43	62.78	64.46	55.09	56.76	45.58	47.18	38.80	40.38	32.28	33.75	23.42	24.77
2003/12/12	55.02	0.44	0.43	62.89	64.57	55.19	56.86	45.65	47.26	38.86	40.45	32.34	33.81	23.46	24.81
2003/12/13	8.49	0.07	0.07	9.71	9.97	8.52	8.78	7.05	7.30	6.00	6.24	4.99	5.22	3.62	3.83
2003/12/14	1.99		0.02	0.00	2.34	0.00	2.06	0.00	1.71	0.00	1.46	0.00	1.22	0.00	0.90

Creation of hourly rainfall data

For calculating hourly rainfall in the above four cases, in order to keep the distribution shape of the respective daily rainfall distributions an interpolation was performed. The interpolation method is outlined below.

- 1) Determine the expected rainfall at the daily boundaries (0:00, 24:00). The day under evaluation and the adjacent days' hourly rainfall (Ph0) are averaged. However, in the case that the day under evaluation or the proceeding day has 0mm rainfall, the corresponding boundary hour's rainfall is set to 0mm. [Exception 1]
 - 2) Based on the basic principle outlined in **Figure II-(1)-6** the hourly rainfall over a 12-hour period is determined. At this point, if the 12-hour hourly rainfall is negative then set the hourly value to 0mm. [Exception 2]
- * If the rainfall data shows an extreme M-shaped pattern then the calculated value may be negative.
- 3) The day under evaluation is divided into morning and afternoon periods.
 - 4) The hourly rainfall in the period from 0:00 to 12:00 is calculated for the morning assuming equally distributed precipitation over the period. (The average value between 0:00 and 12:00). Similarly, the rainfall is calculated for the afternoon period.
 - 5) The proportional distribution of total rainfall for morning and afternoon is set equal to the total one-day rainfall. This step is intended to compensate for the change in overall rainfall resulting from increasing negative rainfall values to 0mm in previous steps.
 - 6) Based on the basic principle (for the morning or afternoon time interval) determine the hourly rainfall at 6:00 and 18:00.
 - 7) Having calculated the expected hourly rainfall at 0:00, 6:00, 12:00, 18:00, and 24:00, use interpolation to calculate hourly rainfall at all other intervals.

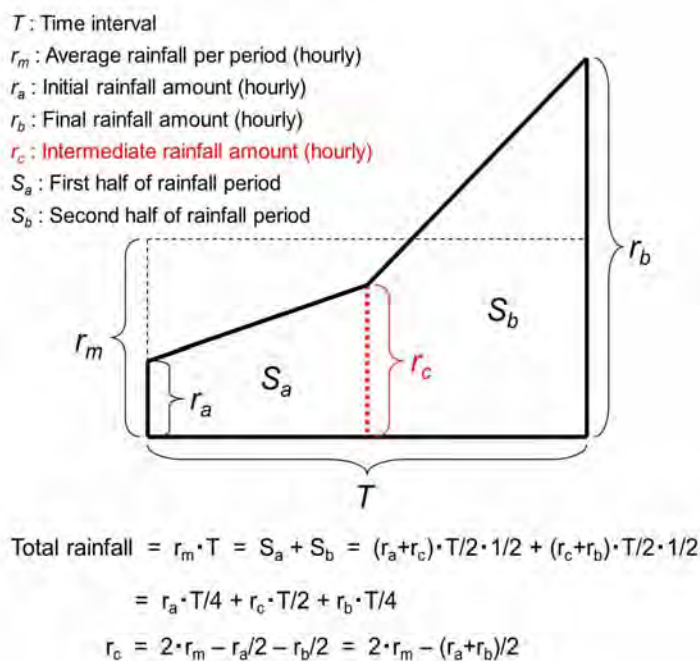


Figure II-(1)-6 Conceptual diagram for interpolation of hourly rainfall

Figure II-(1)-7 shows the simulated rainfall period based on this method.

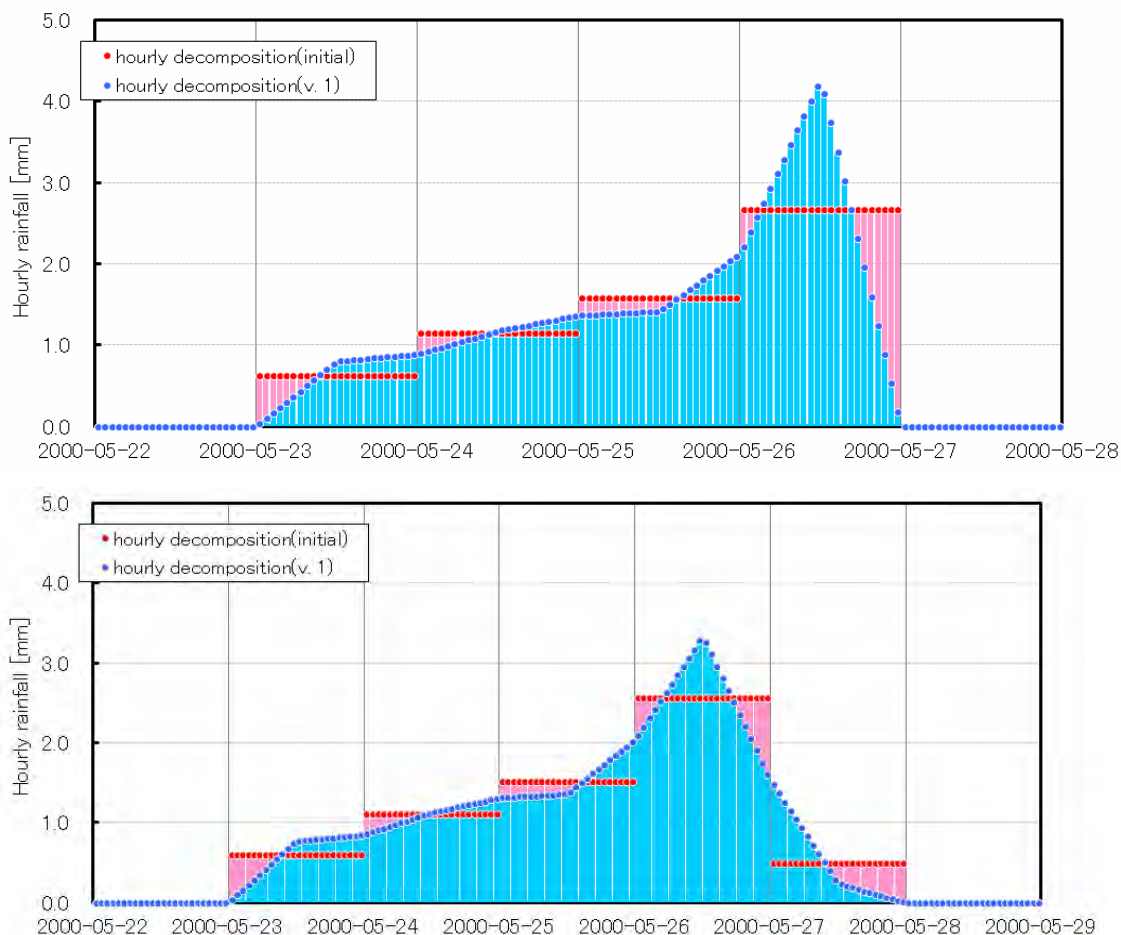


Figure II-(1)-7 Intensity height graph for 2000.5 simulated flood period (above : 4-day rainfall, below : 5-day rainfall)

e. Creation of spatial distribution for expected precipitation data

The rainfall pattern's spatial distribution over the target area varies significantly according to time period, and for the calculation of design flood discharge, it is necessary to take into account this variation. Therefore, gridded rainfall data is interpolated from the observation stations shown in **Figure II-(1)-2** (missing rainfall point data being interpolated from nearest-neighbor observation points). The ratio of grid-point rainfall to overall average daily rainfall for the entire watershed is then calculated. For the four flood cases identified in section *d* above, the estimated each grid daily rainfall is multiplied by the hourly variations of the 4- and 5- day rainfall resulting

in a data grid of temporal and spatial distribution of rainfall. In addition, in order to eliminate discontinuities in spatial distribution at daily temporal boundaries, as shown in **Figure II-(1)-8**, weighted rainfall data from the previous, current, and proceeding days are incorporated at each lattice time interval, and for each return period the precipitation spatio-temporal distribution is created. As one example, **Figure II-(1)-9a to 9d** show the 100-year probability and expected spatial distribution of a continuous four-day rainfall event.

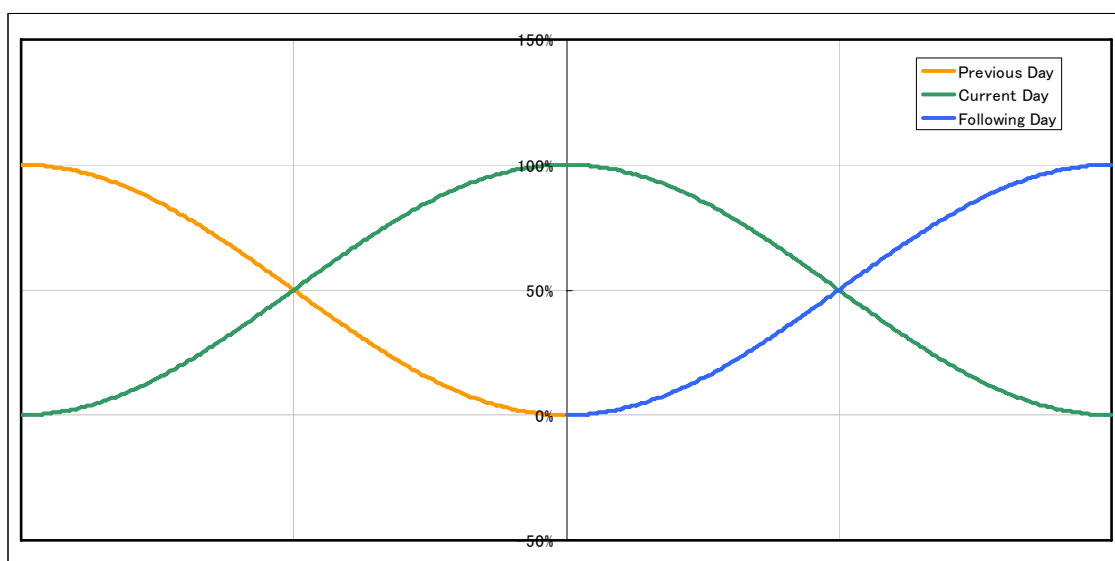


Figure II-(1)-8 Weighting to improve continuity at daily boundary condition

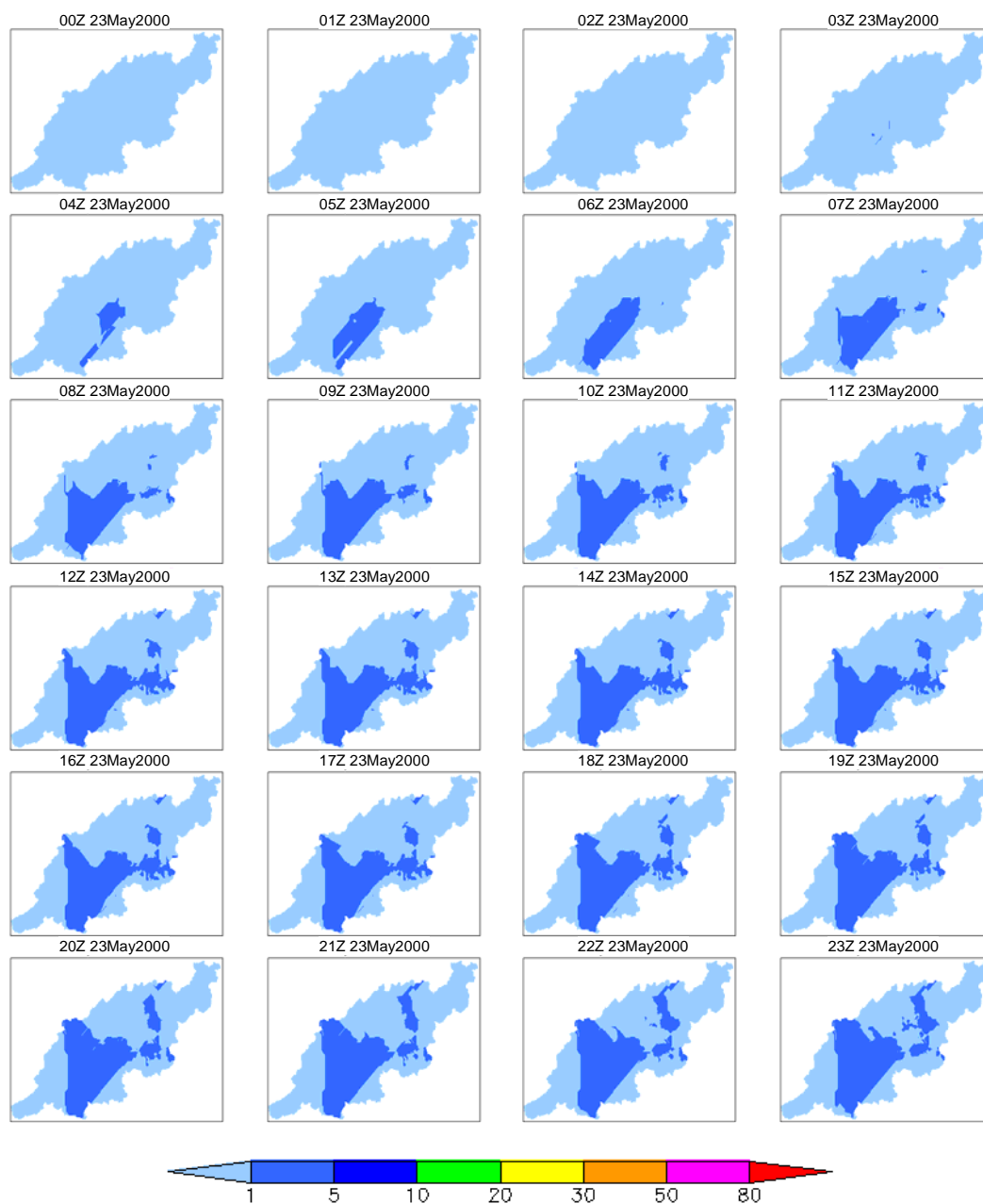


Figure II-(1)-9a 4-day rainfall 100-year prob. spatio-temporal distribution
(May 2000 case, day 1)

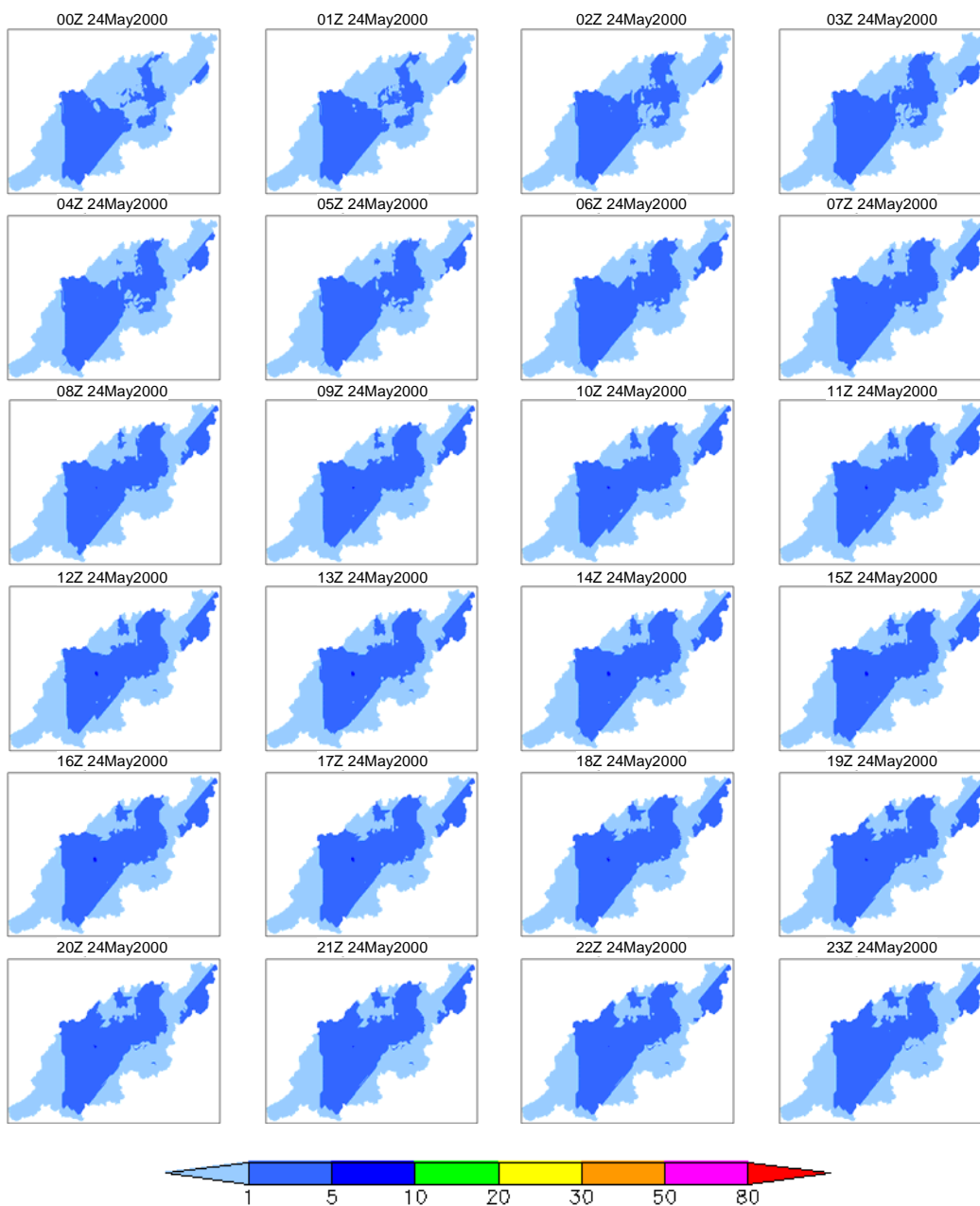


Figure II-(1)-9b 4-day rainfall 100-year prob. spatio-temporal distribution
(May 2000 case, day 2)

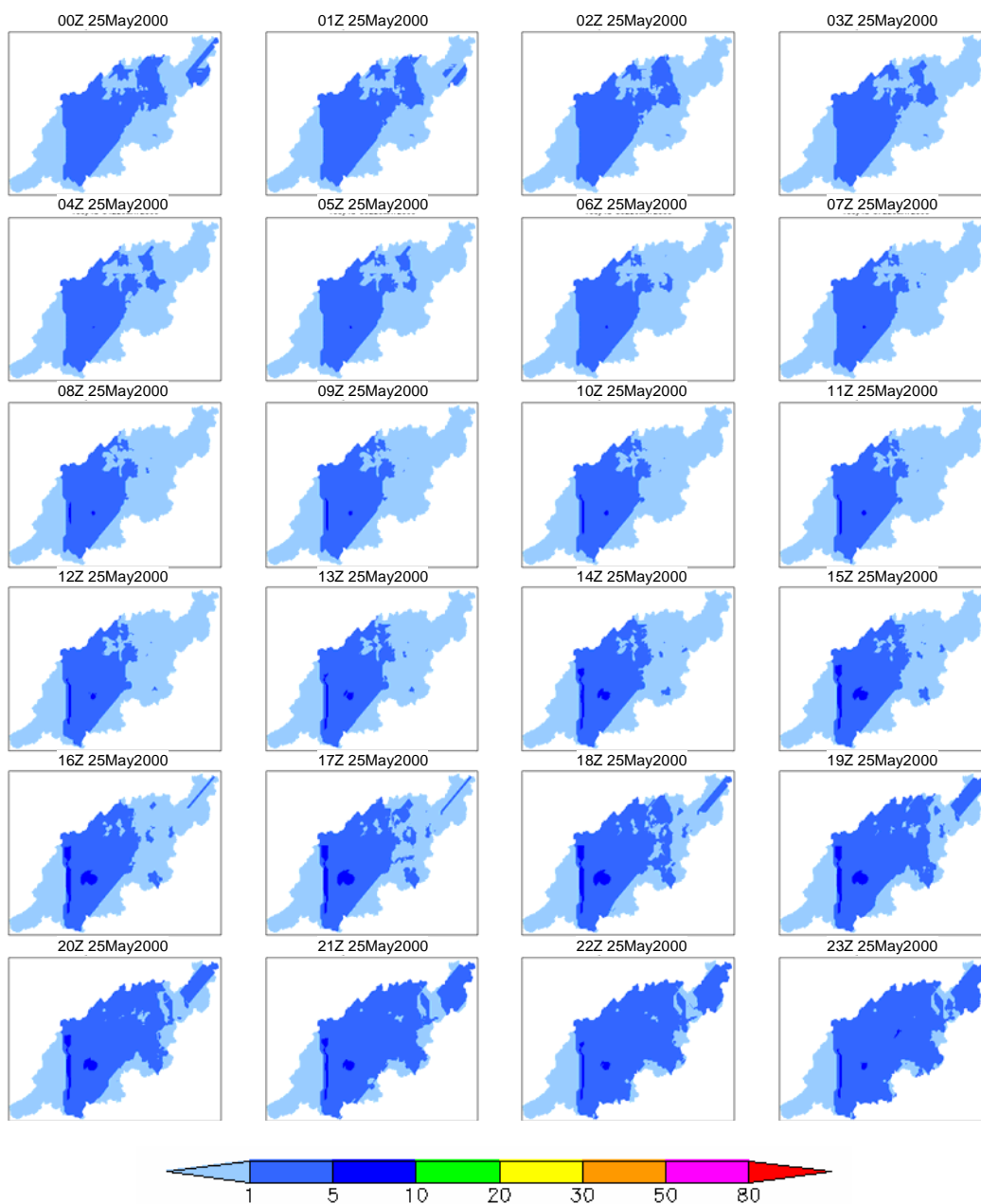


Figure II-(1)-9c 4-day rainfall 100-year prob. spatio-temporal distribution
(May 2000 case, day 3)

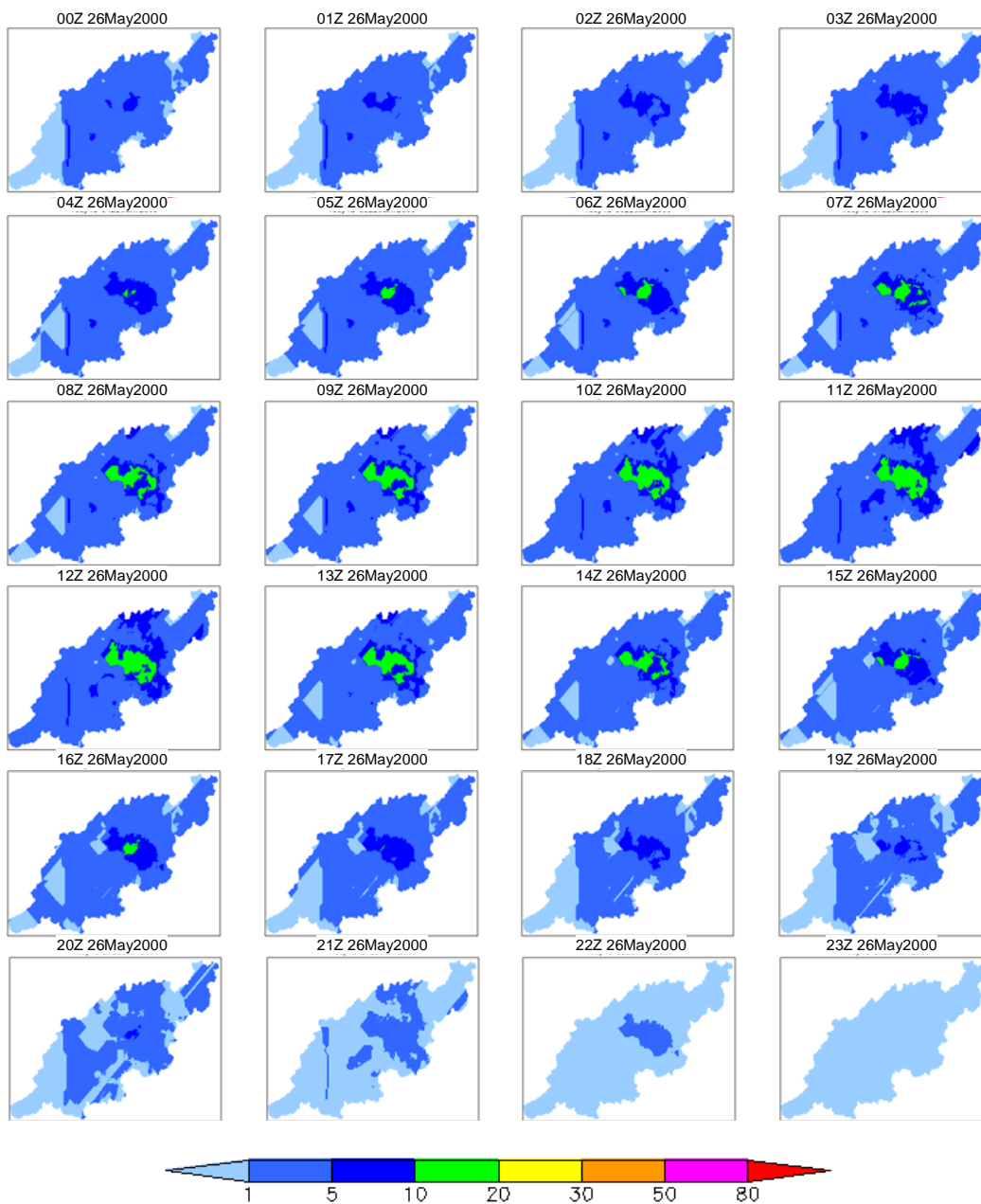


Figure II-(1)-9d 4-day rainfall 100-year prob. spatio-temporal distribution
(May 2000 case, day 4)

2) Design Flood Discharge before Regulation

a. Hydrologic Model Development and Input Data

A distributed hydrological model is an effective tool for simulating slope discharge and river channel flow considering their spatial inhomogeneity from a basin scale to a continental scale. A distributed biosphere hydrological model, the Water and Energy Budget-based Distributed Hydrological Model (WEB-DHM) (Wang et al., 2009), describes the transfer of turbulent fluxes (energy, water, and carbon fluxes) between the atmosphere and land surface for each model grid, and simulates unconfined ground water level and run-off to a river channel in tandem with soil moisture for improving the accuracy of vertical soil water flow and ground water discharge. The WEB-DHM is effectively used in the semi-arid river basin of this study where the water budget between channels and the surrounding areas should be considered in different ways in the alluvial areas and in the others.

Overall Model Structure

The overall model structure is shown in **Figure II-(1)-10** and can be described as follows.

- i. A digital elevation model (DEM) is used to define the target area, after which the target basin is divided into sub basins. Within a given sub basin, a number of flow intervals are specified to represent time lag and accumulating processes in the river network according to the distance to the outlet of the sub basin. Each flow interval includes several model grids.
- ii. Simple Biosphere Model 2 (SiB2) (Sellers et al.,1996) SiB2 is used to calculate turbulent fluxes (water, energy, and CO₂) between the atmosphere and land surface independently. for each model grid with one combination of land use type and soil type.
- iii. Hydrological simulation is done in each model grid consisting of a river channel and a couple of symmetrical hill slopes. By using Geomorphology-Based Hydrological Model (GBHM) (Yang et al., 2000) is used to simulate surface flow, subsurface flow and ground water discharge. For simplicity, the streams located in one flow interval are lumped into a single virtual channel in the shape of a trapezoid. All runoff from the model grids in the given flow interval is accumulated into the virtual channel and led to the outlet of the river basin (**Figure II-(1)-10**).

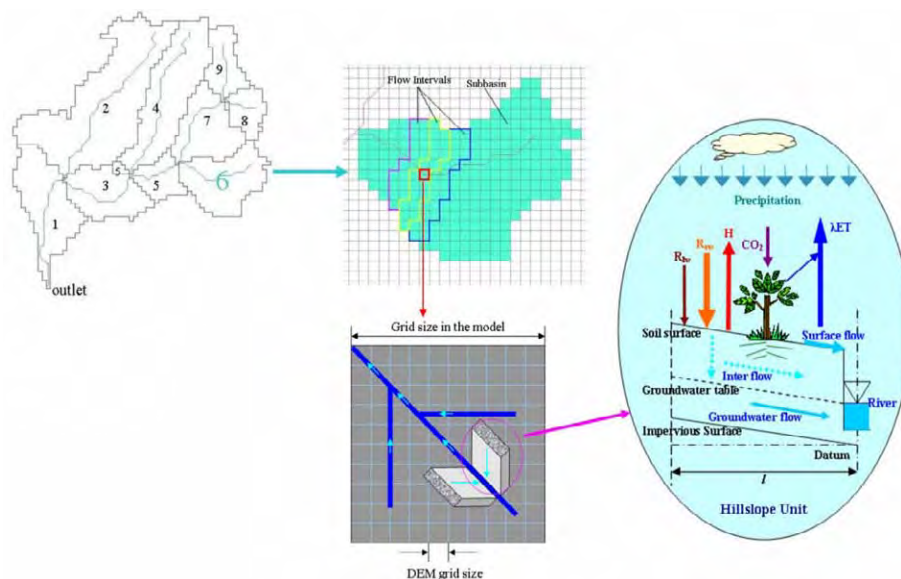


Figure II-(1)-10 Overall Model Structure of the WEB-DHM(Wang et al., 2009)

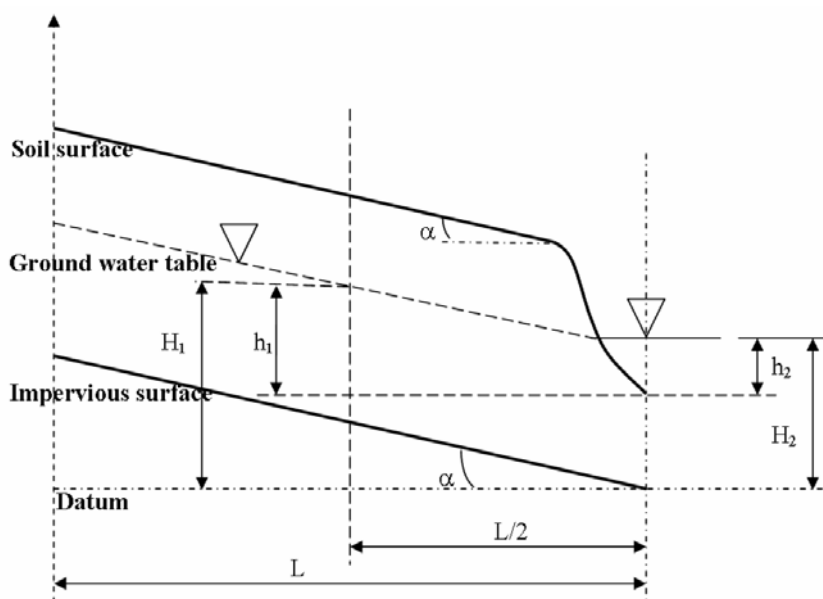


Figure II-(1)-11 Hillslope model (Yang et al., 2000)

Unsaturated and Saturated Zone Water Flows

Sib2 consists of three soil layers; the 1st layer is Surface layer where evaporation is calculated; the 2nd layer is Root Zone where transpiration is calculated; the 3rd layer is Deep Zone which expresses the deepest unsaturated zone. The unsaturated zone water flow is described using a vertical one-dimensional Richards equation:

$$\frac{\partial \theta(z, t)}{\partial t} = - \frac{\partial q_v}{\partial z} + r(z, t) \quad (1)$$

where, t and z are time and depth, respectively; $\theta(z, t)$ is the volumetric water content; $r(z, t)$ is evapotranspiration respectively; q_v is the soil moisture fluxes in the vertical direction, given as

$$q_v = - K(\theta, z) \left[\frac{\partial \psi(\theta)}{\partial z} - 1 \right] \quad (2)$$

where, $K(\theta, z)$ hydraulic constant; $\psi(\theta)$ is capillary suction (m); z is the distance from the surface taken vertically with the downward defined as positive (m).

The basic equations used for the saturated zone are mass balance and Darcy's law. The discharge exchanged between aquifer and river per unit width, $q_G(t)$ calculated as

$$q_G(t) = K_g \frac{H_1 - H_2}{l/2} \frac{h_1 + h_2}{2} \quad (3)$$

where, K_g is the hydraulic conductivity of the unconfined aquifer; l is the length of the hillslope (m); H_1, H_2, h_1, h_2 are in meters (shown in **Figure II-(1)-11**).

Input Data

To develop and evaluate a hydrological model for the Mejerda River Basin, the following data are used:

- River discharge and precipitation: in-situ observation data (observed in Bou Salem and Jendouba during Sep. 2002 through Aug. 2003)
- Atmospheric forcing including air temperature, specific humidity, air pressure, wind speed, downward solar and long wave radiation: long-term reanalysis data by Japanese 25-year Reanalysis Project (JRA25), <http://ds.data.jma.go.jp/gmd/jra/download/download-e.html>
- Landform data: DEM: Hydro1K (USGS): <https://lta.cr.usgs.gov/HYDRO1K>
- Leaf Area Index (LAI) and Fraction of Photosynthetically Active Radiation (FPAR): MODIS: <http://cliveg.bu.edu/modismisr/>
- Land Use Type: Satellite analysis products; United States Geological Survey (USGS): http://eros.usgs.gov/#/Find_Data/Products_and_Data_Available/Land_Cover_Products
- Soil: Digital Soil Data; Food and Agriculture Organization (FAO) <http://www.fao.org/geonetwork/srv/en/metadata.show?id=14116>

b. Model Calibration

The sensitivity check in the target river basin clarifies that permeability is the most sensitive among of the WEB-DHM parameters, including permeability, porosity and asymmetric factor of each soil layer and surface water storage. The WEB-DHM is calibrated by mainly tuning the permeability in the root and deep layers as well as in the surface layer.

Then, the model parameters are tuned in each sub-basin aiming to make the simulated

river discharge to the observed one at Bou Salem and Jendouba from September 2002 to August 2003. Especially, the three flood peaks observed in January 2003 are focused for the model calibration. **Figure II-(1)-12 – Figure II-(1)-15** show the results of the model calibration. The applied data in Figure II-(1)-12 to II -(1)-15 is indicated in the **appendix map 1a-1c**.

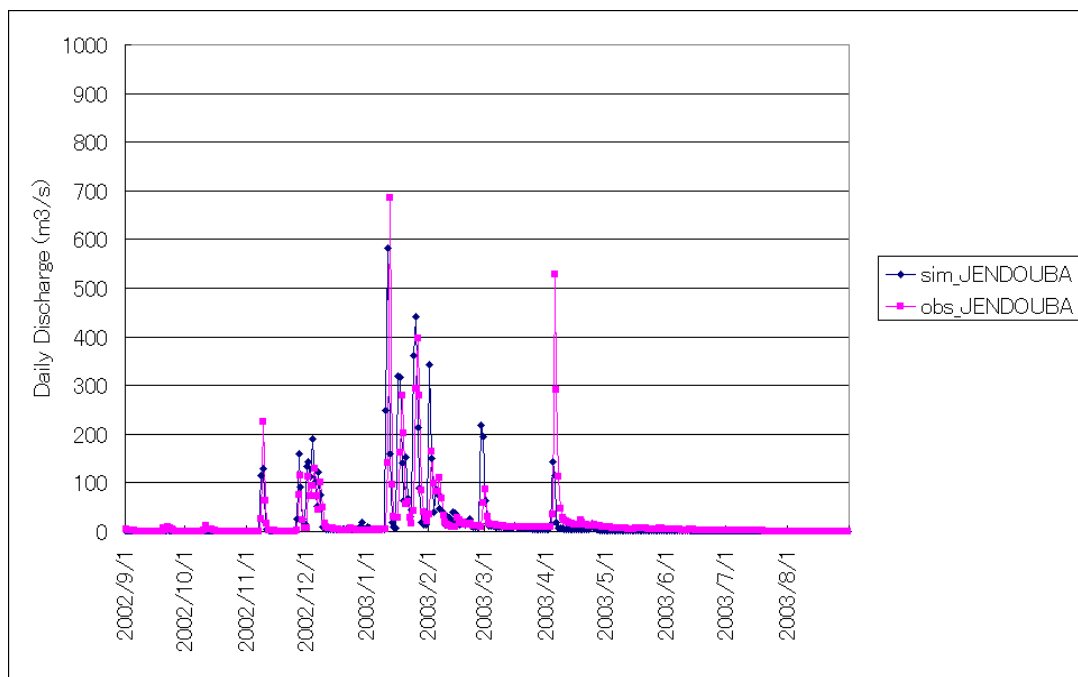


Figure II-(1)-12 Model Calibration at Jendouba from Sept. 2002 to Aug. 2003.

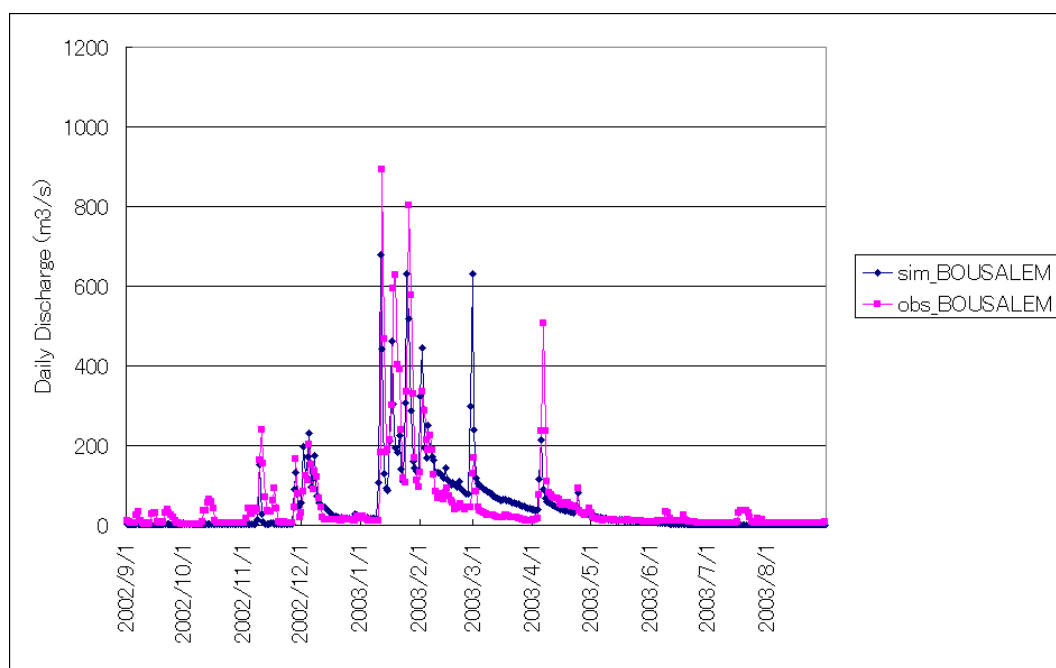


Figure II-(1)-13 Model Calibration at Bou Salem from Sept. 2002 to Aug. 2003.

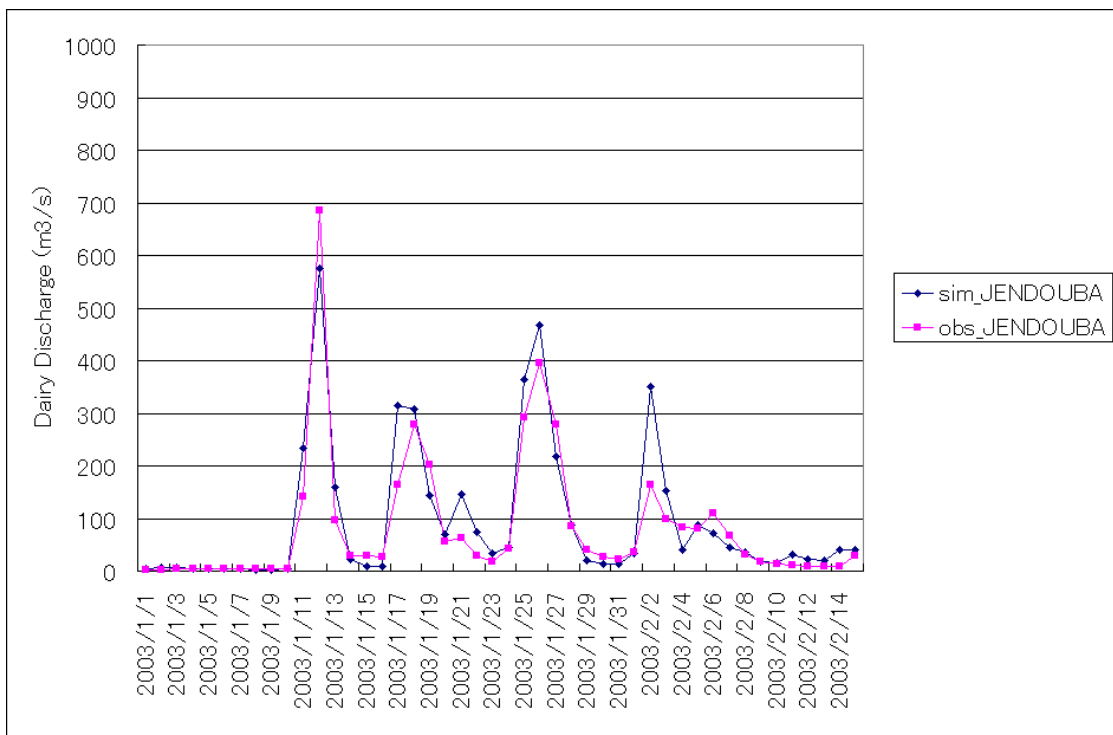


Figure II-(1)-14 Model Calibration at Jendouba during the Flood in January 2003.

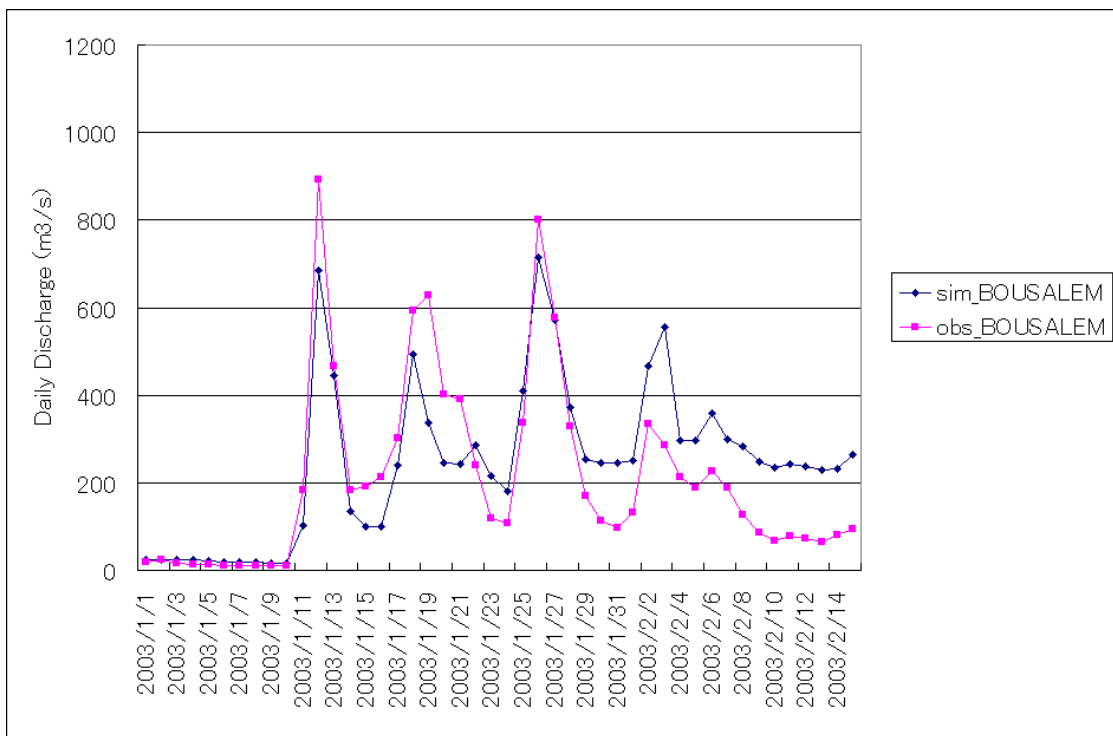


Figure II-(1)-15 Model Calibration at Bou Salem during the Flood in January 2003.

c. Design Rainfall Pattern and Duration

With entered Design rainfall from the past four flood cases (Mar. 1973, May 2000, Jan. 2003, Dec. 2003) into the calibrated WEB-DHM, each flood peak discharge has been compared. The rainfall pattern in May 2000, which results in the highest flood peak among the four cases of each 4-day probability rainfall as shown in **Figure II-(1)-16**, is selected as the design rainfall pattern.

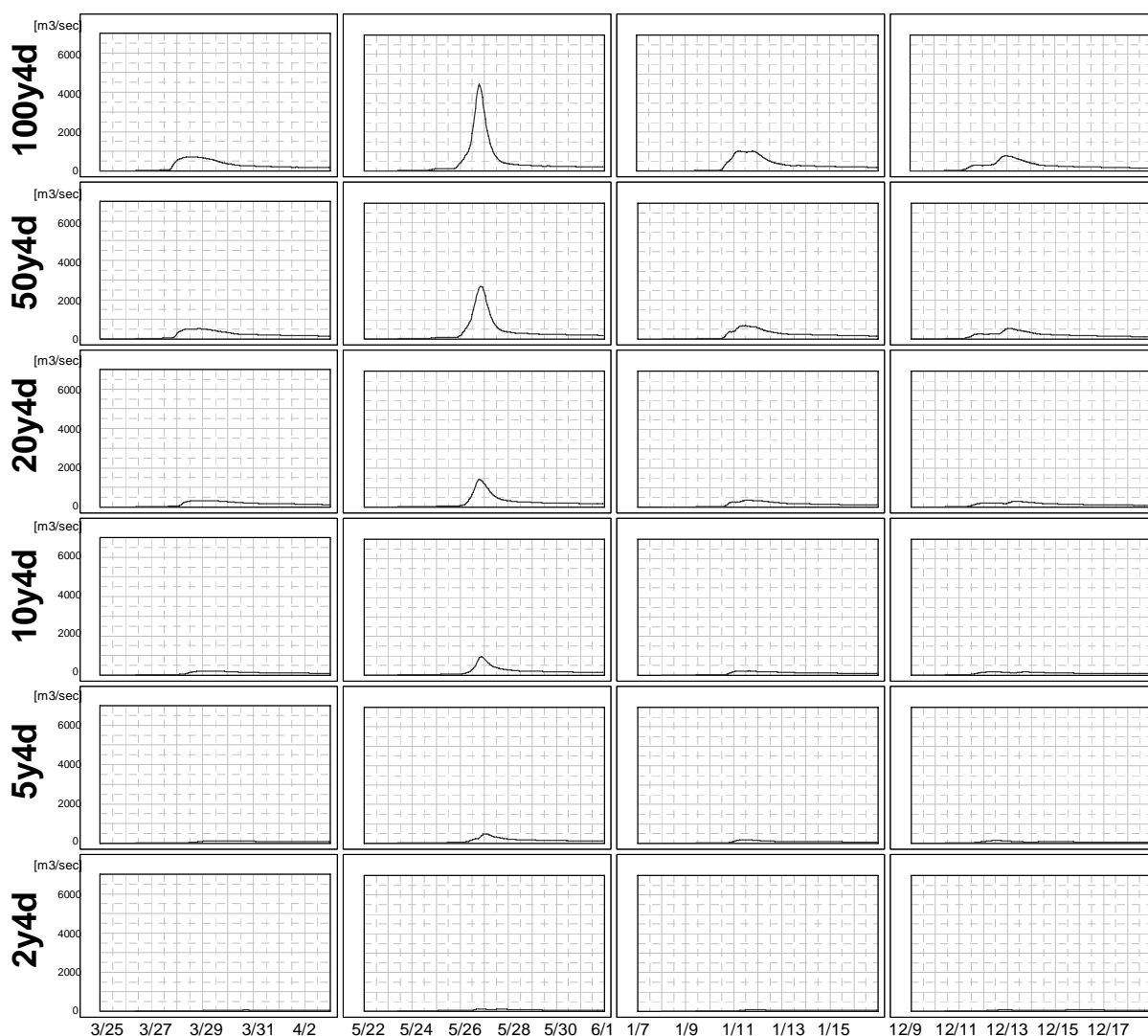


Figure II-(1)-16 Flood Peak Discharge at Sidi Salem Dam with the four Rainfall Patterns of each 4-day probability rainfall (from left, Mar. 1973, May 2000, Jan. 2003, Dec. 2003).(m³/sec)

The higher flood peak with the 4-day rainfall than with 5-day is selected as the design rainfall duration through the comparison at the Sidi Salem dam as shown in in FigureII- (12)-17.

Mejerda River Climate Change Impact Analysis Final Report

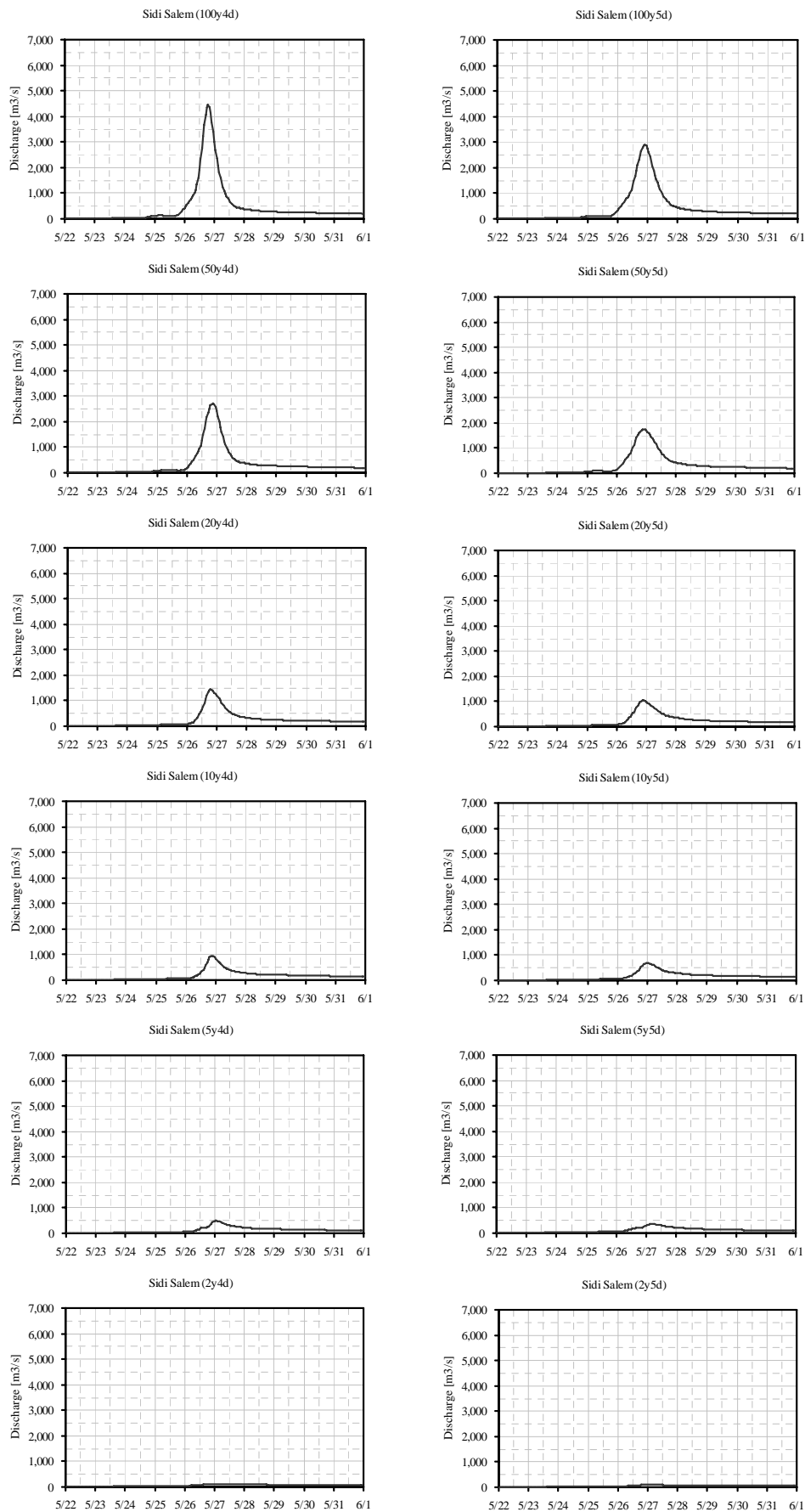


Figure II-(1)-17 The Flood Peaks at the Sidi Salem Dam with the rainfall pattern of May 2000 (left: 4-day rainfall, right: 5-day rainfall)

In conclusion, the design flood discharge is calculated by using 4-day probability rainfall and the rainfall pattern of the flood in May 2000 as shown in **Table II-(1)-5**.

Table II-(1)-5 Design Flood Peak Discharge before Regulation
(The locations are referred to Figure II-(1)-3)

	Design Flood Peak Discharge before Regulation			
	SidiSalem	Larrousia	Chafrou	Siliana
100y4d	4,463	5,707	347	1,547
50y4d	2,717	3,595	136	1,132
20y4d	1,438	1,959	40	650
10y4d	951	1,171	29	375
5y4d	494	552	15	181
2y4d	124	135	0	36

Design flood peak discharge in each observed point is as follows:

Sidi Salem: Flood discharge in Sidi Salem Dam

Larrousia: Flood discharge in Larrousia Dam

Chafrou: Confluence of River Chafrou and Mejerda

Siliana: Confluence of River Siliana and Mejerda

2. Design Flood Discharge after Regulation

1) Introduction of the Sidi Salem Dam Operation

By introducing the following Sidi Salem dam operation, the design flood discharge in the down-stream of the dam is calculated. The following

During the increase phase of the storage water level, it takes six hours to open the lower discharge conduit fully since the storage water level reaches at 116m a.s.l. During decrease phase, it takes two hours to close the lower discharge conduit completely, since the storage water level reaches at 115m a.s.l. In addition, the lower discharge conduit is stopped to open just one step before the full open in case of the 10-year return period.

2) Design Flood Discharge after the Sidi Salem Dam Operation

The design flood discharge for each return period is calculated at the three points in the down-stream of the Sidi Salem dam by introducing the release from the dam as shown in **Figure II-(1)-18** and Table II-(1)-6.

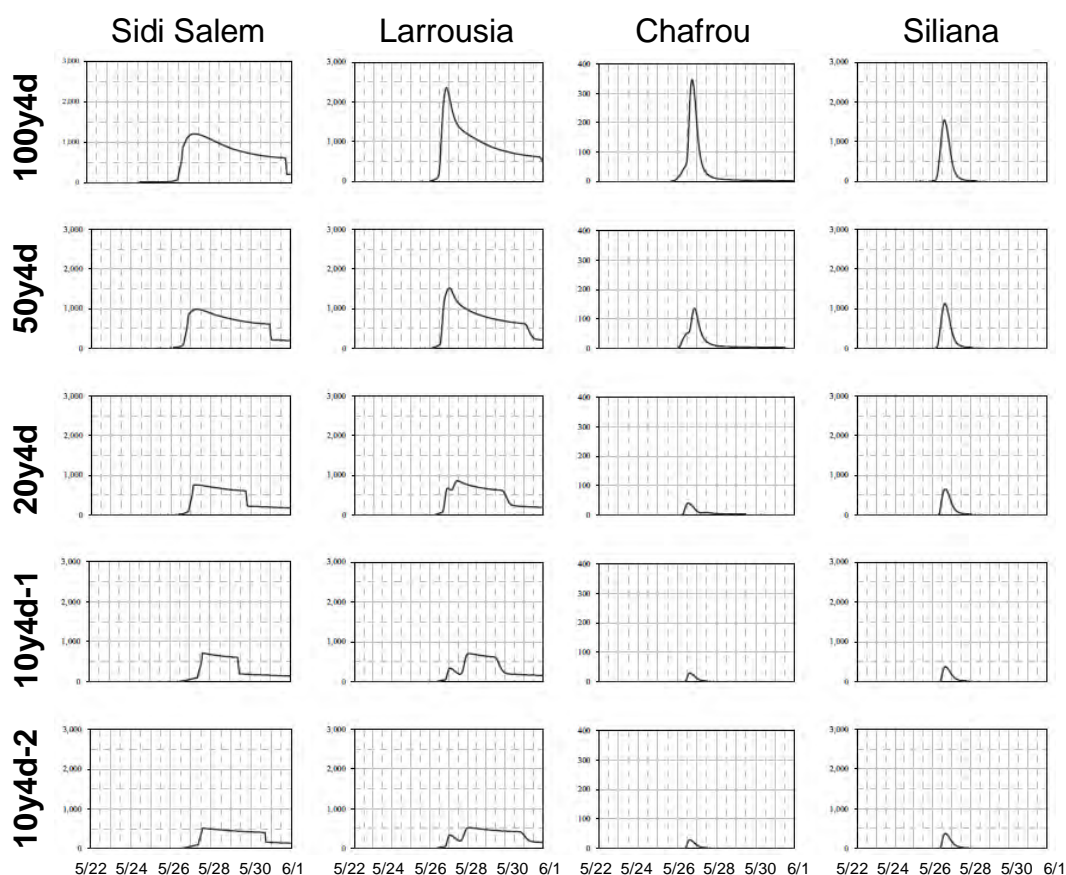


Figure II-(1)-18 Design Flood Discharge after Regulation and the Dam Release(m^3/sec) from left, Sidi Salem, Larrousia, Chafrou, Siliana, and from top, 100y4d, 50y4d, 20y4d, 10y4d-1(full open), 10y4d-2 (stopped at just one step before the full open)

As a result from above mentioned, each design flood peak discharge corresponding to each return period is shown in the **Table II-(1)-6**.

Table II-(1)-6 Design Flood Peak Discharge after Regulation
(The locations are referred to Figure II-(1)-3)

	Design Flood Peak Discharge after Regulation			
	SidiSalem	Larrousia	Chafrou	Siliana
100y4d	1,202	2,361	347	1,547
50y4d	980	1,517	136	1,132
20y4d	754	859	40	650
10y4d-1	713	706	29	375
10y4d-2	516	522	29	375

(2) Climate Change Impact Assessment of the Mejerda River Basin

The framework of the climate change analysis is shown in **Figure II-(2)-1**. There are five components as follows:

1. Selection of the Emission Scenario
2. GCM Selection
3. Bias Correction of the Rainfall from the Selected GCMs
4. Assessment of Changes in Rainfall
5. Assessment of Changes in the Design Floods

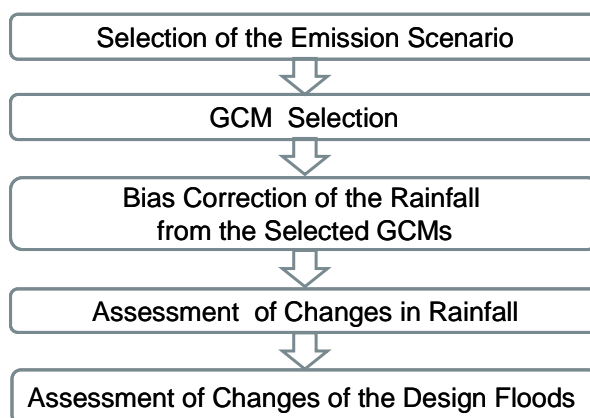


Figure II-(2)-1 Framework of the Climate Change Analyses

1. Selection of the Emission Scenario

The Special Report on Emission Scenarios (SRES), published by the IPCC in 2000, describes the emissions scenarios that have been used to make projections of possible future climate change, for the IPCC Third Assessment Report (TAR) and in the IPCC Fourth Assessment Report (AR4). Emission scenarios describe future releases of greenhouse gases, aerosols, and other pollutants in the atmosphere, along with information on land use and land cover. A set of four scenario families (A1, A2, B1, B2) have been developed. Each of these scenarios describes one possible demographic, socio-economic, political and technological future. The SRES A1B scenario is selected as our GCM in this study. This is under the A1 storyline and the scenario family describing a future world with very rapid economic growth, global population that peaks in the mid-century and declines thereafter, and with the rapid introduction of new and more efficient technologies. The A1B scenario considers a balance across all sources (the term “balanced” here is defined as not relying too heavily on one particular energy source, on the assumption that similar improvement rates apply to all energy supply and end-user technologies). This scenario is characterized by low population growth, very high GDP growth, very high energy

use changes, medium resource availability and rapid but balanced pace and direction of technological change (IPCC Working Group III, 2000).

2. GCM Selection

GCM Selection is done based on the ability of representing the regional climate of the subject area. If a GCM is not able to reproduce the current climatology of the surveyed region, it should not be considered for any further examinations. The selection of the domain is based on these broad synoptic scale phenomena. The climate systems unique to the basins as well as the spatial coverage should be applied for the evaluation.

On a basin scale, the selected GCMs should be able to reproduce the seasonal pattern of precipitation. Spatial correlation (Scorr) and the root mean square error (RMSE) were used to identify similarities and differences between the models versus current observed global datasets. The Global Precipitation Climatology Project (GPCP) dataset was used for comparing similarities in average monthly precipitations while the Japan Reanalysis data (JRA25) output was used to compare other meteorological variables.

$$Scorr = r_{xy} = \frac{\sum_{i=1}^N (x_i - \bar{x})(y_i - \bar{y})}{(n-1)S_x S_y} = \frac{\sum_{i=1}^N (x_i - \bar{x})(y_i - \bar{y})}{\sqrt{\sum_{i=1}^N (x_i - \bar{x})^2 \sum_{i=1}^N (y_i - \bar{y})^2}} \quad (4)$$

$$RMSE = \sqrt{\frac{1}{N} \sum_{i=1}^N (R_{si} - R_{obs})^2} \quad (5)$$

To evaluate the GCMs' ability to represent the small-scale precipitation, additional screening should be done to eliminate the worst performing GCMs. Three additional screening criteria were applied for this elimination:

- a) The long term basin observed rainfall average (climatology) should be compared to the GCMs. If a GCM is not able to represent the seasonal variability, then it should be eliminated.
- b) If a GCM produces a trace of rainfall even after the no-rain correction has been done where unreasonably dry days exist; then that model should also be eliminated.
- c) Lastly, if the observed rainfall distribution within the basin is not uniformly distributed, consideration on basin subdivision climatological average (based on areas with high rainfall, medium rainfall, small rainfall –usually related to elevation and land use) should be considered in the model selection comparison.

Selection of GCMs among available models in the Coupled Model Inter-comparison Project 3 (CMIP3) is crucial for this multi-model analysis. There are 7 parameters, including precipitation, outgoing longwave radiation, sea level pressure, meridional wind and zonal wind, sea surface temperature, and air temperature, as shown in **Table II-(2)-1**, considered in selecting the

appropriate GCMs that comprises the ensemble.

The data and the tools used in this study are provided by the CMIP3 data and some other software tools such as model evaluation, model selection, and data downloading methods which have been developed on the Data Integration and Analysis System (DIAS) system.

Table II-(2)-1 Target season, Temporal scale and parameters for the GCM selection

Parameter	Target Season	Region Scale	Local Scale
Precipitation	Winter (Oct – Jan)		5°E- 15°E 25°N – 39°N
Outgoing Long wave radiation	Winter (Oct – Jan)		5°E- 15°E 25°N – 39°N
Sea level Pressure	Winter (Oct – Jan)	30°W- 50°E 20°N – 50°N	
Meridional wind	Winter (Oct – Jan)	30°W- 50°E 20°N – 50°N	
Zonal wind	Winter (Oct – Jan)	30°W- 50°E 20°N – 50°N	
Sea Surface Temperature	Summer (May – Aug)	30°W- 50°E 20°N – 50°N	
Air Temperature	Summer (May – Aug) Winter(Oct – Jan)		5°E- 15°E 25°N – 39°N

The area considered for local scale meteorological parameter (precipitation) is 5°E to 15°E, 25°N to 39°N, and the area for large scale circulations and surrounding oceans is designated as 30°W to 50°E; 20°N to 50°N as shown in **Figure II-(2)-2**.

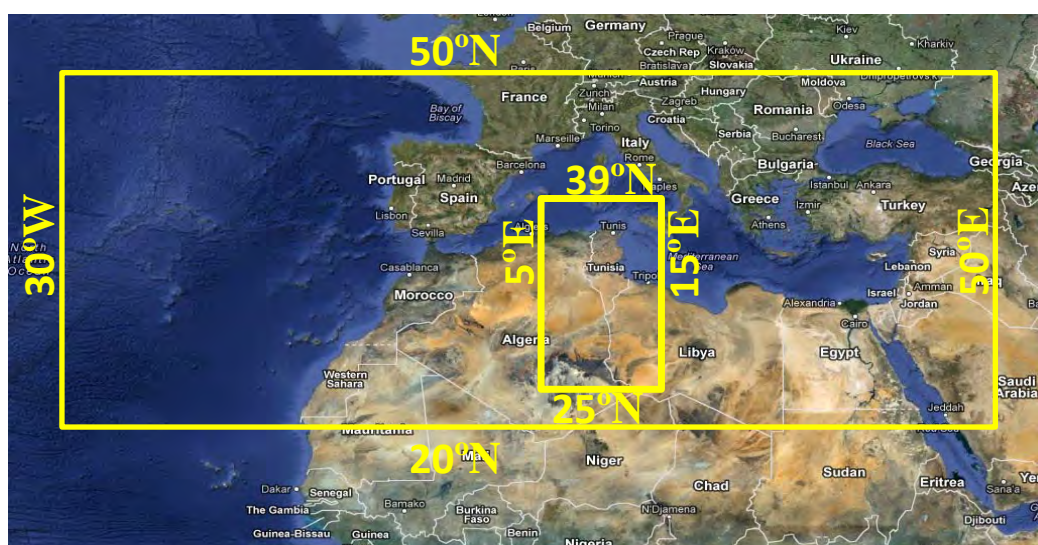


Figure II-(2)-2 Target region for the GCM selection

A simple index counter was used for identifying the models which had Scorr and RMSE values above the average Scorr and RMSE (if above average, index = 1, else index = 0). Within the top ten models selected by using the 7 parameters as shown in **Table II-(2)-2**, two models, ukmo_hadgem1 and gfdl_cm2_1, were excluded due to their worse performance of the expression of precipitation in the wet season as shown in the **Table II-(2)-3**. Due to the incomplete data set availability, neither bccr_bcm20 nor ukmo_hadcm3 were included in this study.

Table II-(2)-2 The top ten models selected by using the 7 parameters

No	GCM Ranking	5E-15E		30W-40E		30W-40E		5E-15E		Grand Total Index
		25N-39N	25N-39N	20N-50N	20N-50N	20N-50N	20N-50N	25N-39N	25N-39N	
1	bccr_bcm2_0	1	1	0	1	1	1	1	1	7
2	cccma_cgcm3_1	1	1	0	1	1	1	0	1	6
3	ingv_echam4	0	0	1	1	1	1	0	1	5
4	miroc3_2_hires	1	0	1	0	1	0	1	1	5
5	mpi_echam5	0	0	1	1	1	1	1	0	5
6	ukmo_hadcm3	1	1	1	0	1	1	0	0	5
7	ukmo_hadgem1	-1	1	1	1	1	1	1	0	5
8	cccma_cgcm3_1_t63	1	0	0	0	1	1	0	0	3
9	gfdl_cm2_1	-1	1	1	1	0	0	0	1	3
10	mri_cgcm2_3_2a	0	1	1	1	1	0	0	-1	3
11	gfdl_cm2_0	1	0	0	-1	0	0	1	0	1
12	giss_model_e_r	0	1	0	-1	0	0	1	0	1
13	miroc3_2_medres	0	1	0	1	0	0	0	-1	1
14	cnrm_cm3	0	0	-1	-1	0	0	1	1	0
15	giss_model_e_h	0	1	-1	0	0	-1	0	1	0
16	miub_echo_g	1	0	0	-1	0	0	0	0	0
17	ncar_ccsm3_0	0	1	-1	-1	0	0	0	1	0
18	csiro_mk3_5	-1	-1	-1	1	0	0	1	0	-1
19	csiro_mk3_0	-1	0	-1	0	1	0	-1	-1	-3
20	giss_aom	-1	0	-1	0	-1	-1	0	1	-3
21	inmcm3_0	-1	0	-1	0	-1	-1	0	1	-3
22	ipsl_cm4	0	0	-1	0	0	-1	0	-1	-3
23	ncar_pcm1	0	0	-1	0	-1	-1	0	-1	-4
24	iap_fgoals1_0_g	0	0	-1	-1	-1	-1	0	-1	-5

Table II-(2)-3 The scoring at wet season

model	5E-15E & 25N-39N		Oct		Nov		Dec		Jan		Average 4 month		S_corr Index	RMSE Index	Total Index Precip
	S_corr	RMSE	S_corr	RMSE	S_corr	RMSE	S_corr	RMSE	S_corr	RMSE	S_corr	RMSE			
1	bccr_bcm2_0	0.96672	0.24326	0.96444	0.37114	0.90929	0.51771	0.86463	0.577913	0.92677025	0.427508	1	1	1	
2	cccma_cgcm3_1	0.96676	0.20113	0.95024	0.38398	0.92669	0.36117	0.90249	0.348677	0.93654425	0.3237375	1	1	1	
3	cccma_cgcm3_1_t63	0.96752	0.21654	0.96038	0.28705	0.94855	0.35204	0.90318	0.362201	0.94490775	0.30445575	1	1	1	
4	cnrm_cm3	0.86434	0.38458	0.9363	0.51278	0.90315	0.63841	0.84625	0.598258	0.887511	0.533507	0	1	0	
5	csiro_mk3_0	0.92652	0.46213	0.90261	0.68082	0.83501	0.66315	0.76123	0.705902	0.856343	0.6279985	0	0	-1	
6	csiro_mk3_5	0.88431	0.63161	0.85477	0.78266	0.79394	0.70339	0.69582	0.736808	0.8072085	0.71361725	0	0	-1	
7	gfdl_cm2_0	0.94633	0.25597	0.96329	0.34793	0.89737	0.56844	0.85395	0.488814	0.9152345	0.415287	1	1	1	
8	gfdl_cm2_1	0.89816	0.53141	0.92648	0.73926	0.86869	0.78988	0.77901	0.666212	0.8680865	0.681691	0	0	-1	
9	giss_aom	0.90472	0.41939	0.90955	0.67065	0.9057	0.63434	0.85113	0.642466	0.89277175	0.59171075	0	0	-1	
10	giss_model_e_h	0.84383	0.5915	0.92515	0.42553	0.8962	0.42831	0.85166	0.439001	0.87921125	0.47108475	0	1	0	
11	giss_model_e_r	0.847	0.67726	0.88605	0.47348	0.9093	0.39966	0.88084	0.408311	0.8807955	0.489677	0	1	0	
12	iap_fgoals1_0_g	0.95457	0.57582	0.92503	0.65602	0.90999	0.61532	0.87582	0.63443	0.916352	0.6203975	1	0	0	
13	ingv_echam4	0.92901	0.55898	0.95203	0.55458	0.92246	0.6893	0.90557	0.594831	0.9272675	0.59942225	1	0	0	
14	inmcm3_0	0.94487	0.59185	0.85366	0.96564	0.88449	0.83999	0.86181	0.722015	0.8862075	0.7798755	0	0	-1	
15	ipsl_cm4	0.9166	0.69832	0.87238	1.00189	0.91362	0.92208	0.91169	0.74262	0.90357475	0.84122675	1	0	0	
16	miroc3_2_hires	0.88981	0.49489	0.97874	0.21243	0.96324	0.28352	0.95752	0.285954	0.94732775	0.319198	1	1	1	
17	miroc3_2_medres	0.90762	0.37245	0.94492	0.58999	0.90741	0.70287	0.85413	0.677073	0.90351975	0.58559575	1	0	0	
18	miub_echo_g	0.93605	0.33656	0.94933	0.37966	0.92565	0.55765	0.89445	0.592521	0.92636825	0.46659675	1	1	1	
19	mpi_echam5	0.90883	0.40746	0.93518	0.51303	0.89236	0.6853	0.79993	0.573776	0.88407275	0.54489225	0	1	0	
20	mri_cgcm2_3_2a	0.91446	0.49038	0.93822	0.65917	0.92151	0.79298	0.84277	0.569821	0.90423925	0.62808575	1	0	0	
21	ncar_ccsm3_0	0.93857	0.37967	0.94462	0.62965	0.91634	0.66505	0.89861	0.614014	0.924538	0.57209675	1	0	0	
22	ncar_pcm1	0.98076	0.25267	0.94725	0.68616	0.91448	0.727	0.88475	0.637442	0.926806	0.57831825	1	0	0	
23	ukmo_hadcm3	0.97537	0.31166	0.97109	0.27328	0.94985	0.41353	0.89013	0.443964	0.94661075	0.36060875	1	1	1	
24	ukmo_hadgem1	0.92952	0.75825	0.87507	0.7476	0.87166	0.51808	0.86614	0.500818	0.8859925	0.631182	0	0	-1	

Finally, 6 models were selected for this evaluation. They are: cccma_chcm31, cccma_chcm31_t63, miroc32_hires, mpi_echam5, mri_cgcm23_2, ingv_echam4. **Figure II-(2)-3** shows how the spatial distribution of rainfall over the region for the selected 6 models indicates similar patterns as those of GPCP for the wet season from October to January.

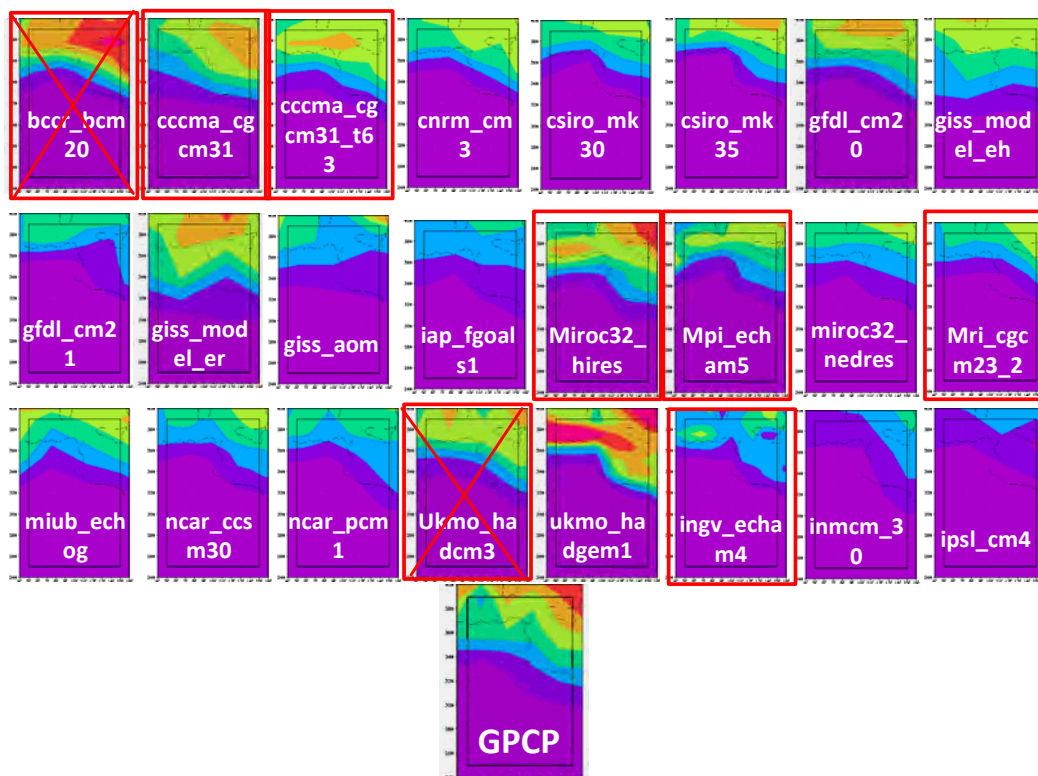


Figure II-(2)-3 The spatial distribution of rainfall over the region

3. Bias Correction of the Rainfall from the Selected GCMs

Precipitation outputs from the GCMs cannot be directly used to force hydrological or other impact assessment models when seeking a realistic output without some form of prior bias correction (Ines and Hansen, 2006, Feddersen and Andersen, 2005, Sharma et al., 2007). If used directly, it may magnify the errors resulting from these biases. Hence, it is necessary to correct the biases prior to utilization of model outputs. To utilize GCM scenario outputs in a hydrological study, an appropriate downscaling is needed. Two downscaling approaches are typically available; statistical downscaling and dynamical downscaling. Dynamic downscaling involves the use of finer resolution numerical weather prediction models with GCM output as initial and boundary conditions. Statistical downscaling involves the use of statistical relationships to convert the large-scale projections from GCM to higher spatial resolutions. This part of the report presents the necessary steps to achieve a simplified statistical approach based on statistics.

To achieve a reasonable bias correction for precipitation, it is required to separate no-rain days from normal rain days and from extreme rain days. Due to the threshold ability of the incorporated parameterization schemes in their simulations; GCMs output are characterized by many wet days (with lots of drizzle) and they do not represent extreme events so precisely. This necessitates the separation of these three types of rainfall events. To account for the basins with extremely distinct seasons (e.g. very dry and wet seasons); bias correction should be performed individually by each season. This should be done at a monthly or a bi-monthly scale depending on the basin climatology.

Bias correction using this approach is a three step process, including extremely heavy rain days, no rain days and normal rain days, as shown in **Figure II-(2)- 4** (Nyunt, et al., 2012).

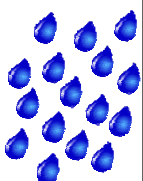
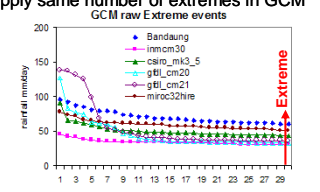
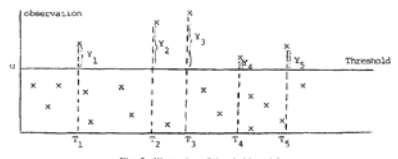

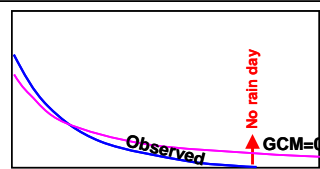
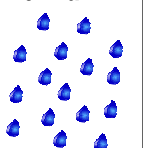
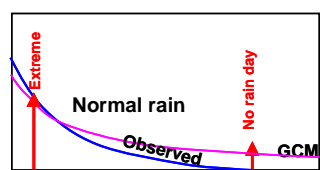
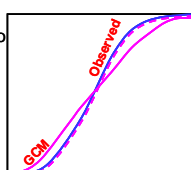
Rain Type	Threshold	Correction
Extreme 	<ul style="list-style-type: none"> - Larger than minimum of annual maxima of station - count the number of extreme events in station (eg. Top of 30 rainfall by ranking all rainfall) - apply same number of extremes in GCM 	Generalized Pareto Distribution <ul style="list-style-type: none"> -Non every year statistics -Extreme (long or short tailed) fitting -Peak over threshold method  <p>Fig. 2. Illustration of threshold model.</p>
No rain day 		Ranking order statistics <ul style="list-style-type: none"> - frequency of no rain day in GCM is same as station - less than no rain day threshold change zero rainfall.
Normal 		Gamma Distribution <ul style="list-style-type: none"> - monthly CDF of GCM mapping to monthly CDF of station - inverse of Gamma CDF in each month is corrected rain 

Figure II-(2)-4 Bias correction approach using three step process

STEP 1: Extreme rainfall correction

Most of the GCMs underestimate extreme rainfall compared to observations. To account for this, appropriate correction should be applied to adjust these values to match the distribution by observations.

Annual maxima rainfall was selected for each year in the observed dataset. The lowest value of the annual maxima was selected as the threshold of the extreme events for observed rainfall.

Values above this threshold are defined as extreme events. The number of extreme events are determined from observed stations and set with the same number of extreme events in past GCMs by ranking. Above this threshold the General Parieto Distribution (GPD) was fitted into the data. The GPD is the limit distribution of excess over a threshold series. The GP distribution function is

$$F(x) = 1 - \left[1 - \frac{\kappa(x - \xi)}{\alpha} \right]^{1/\kappa} \quad (6)$$

where κ is the shape parameter, α is the scale parameter, and ξ is the location parameter estimated by the moment estimators via the following equations.

$$\alpha = \frac{1}{2} \mu \left(\frac{\mu^2}{\sigma^2} + 1 \right) \quad (7)$$

$$\kappa = \frac{1}{2} \left(\frac{\mu^2}{\sigma^2} - 1 \right) \quad (8)$$

where μ is the sample mean and σ^2 the sample variance. ξ is the location parameter and is estimated by checking the sensitivity of ξ to κ . After bias-correction was done for control and projection periods, recurrences of maximum extreme events X_T for different return periods of T years was estimated using

$$X_T = \xi + \frac{\alpha}{\kappa} \left[1 - (\lambda T)^{-\kappa} \right] \quad (9)$$

where λ is the average number of events per year above the threshold.

STEP 2: No-rain day correction

A common characteristic of all GCMs is unrealistically high number of wet days. Most of these cases are represented as drizzle and they attribute to lack of parameterization in GCMs. To correct this defect, the method below is employed.

- a) Both past observations and GCM extracted values are ranked in descending order.
- b) A threshold of 0 mm/day was considered for no-rain day in the observations. The rank of this threshold is then used to determine the corresponding value of no rain day in the GCMs
- c) All values equal or below this rank in the GCM is equated to zero
- d) No-rain day correction for the future GCM is based on the threshold for past GCMs

STEP 3: Normal rainfall correction

Normal rainfall is in the range between zero rainfall and the extreme rainfall. Correction

in this band is based on the gamma distribution function (eq.10) fitted to past observations and GCMs.

$$F(x; \alpha, \beta) = \frac{1}{\beta^\alpha \Gamma(\alpha)} x^{\alpha-1} \exp\left(-\frac{x}{\beta}\right); x \geq 0 \quad (10)$$

where α and β are shape and scale parameters for the gamma distribution, determined by the methods of moment estimation. The inverse of the gamma distribution for past observed rainfall is used to correct for past GCM rainfall. This is then used as a transfer function for the future normal rainfall correction.

Spatial Downscaling was done by correcting the biases on each of the 44 rainfall gauge data. **Figure II-(2)-5** shows the distribution of the gauge stations that were bias corrected for this study. After bias correction of the GCM outputs, a method of inverse proportion to square of distance is used to get a grided distribution map of the bias-corrected GCM outputs.

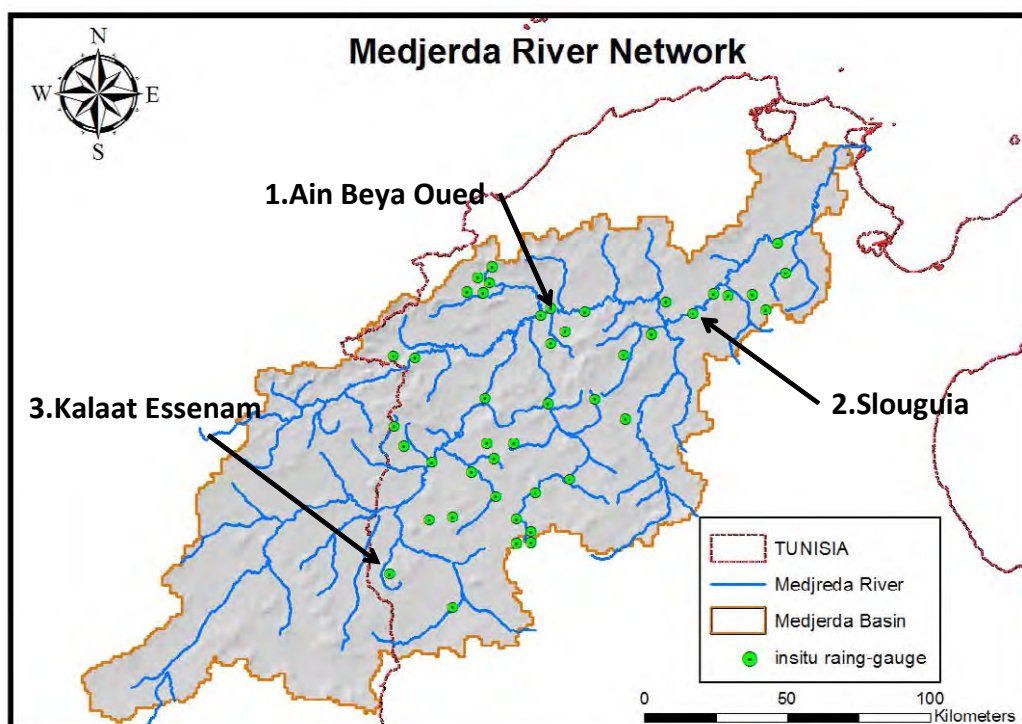


Figure II-(2)-5 The distribution of the rain gauge stations at Medjerda river basin

Figure II-(2)-6, 7, 8 show the monthly average rainfalls and the top seventy daily rainfalls of the rank order statistics from 1981 to 2000 before (left) and after (right) the bias-corrections at Ain Beya Oued in the middle of the basin where the largest amount of rain happens, Slouguia in the downstream, and Kalaat Essesnam in the upstream which are the driest points in the basin, respectively.

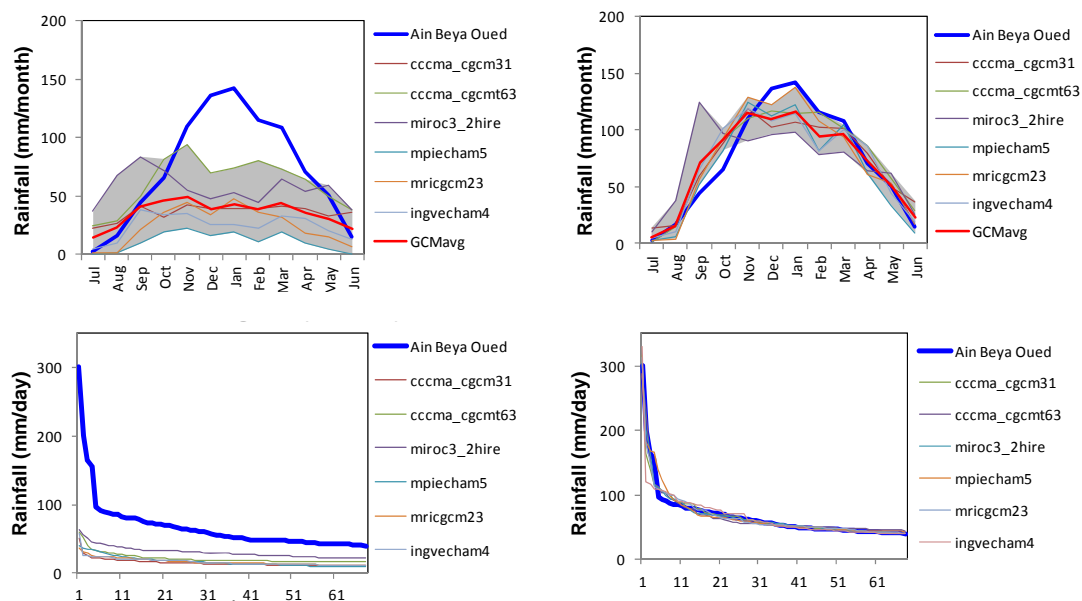


Figure II-(2)-6 The monthly average rainfalls and the extremely heavy top seventy daily rainfalls before (left) and after (right) the bias-corrections at Ain Beya Oued

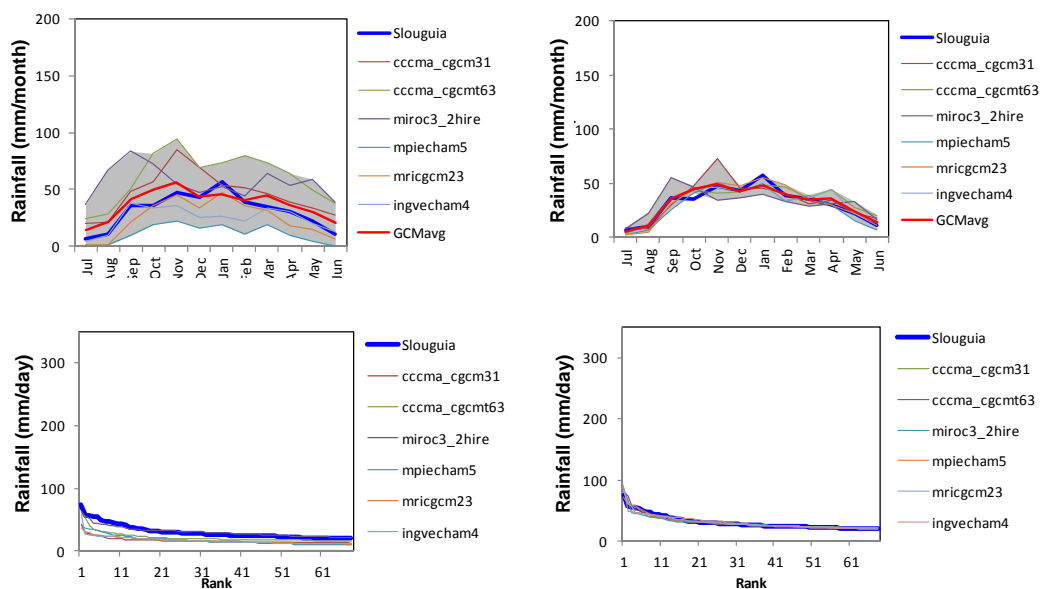


Figure II-(2)-7 The monthly average rainfalls and the extremely heavy top seventy daily rainfalls before (left) and after (right) the bias-corrections at Slouguia

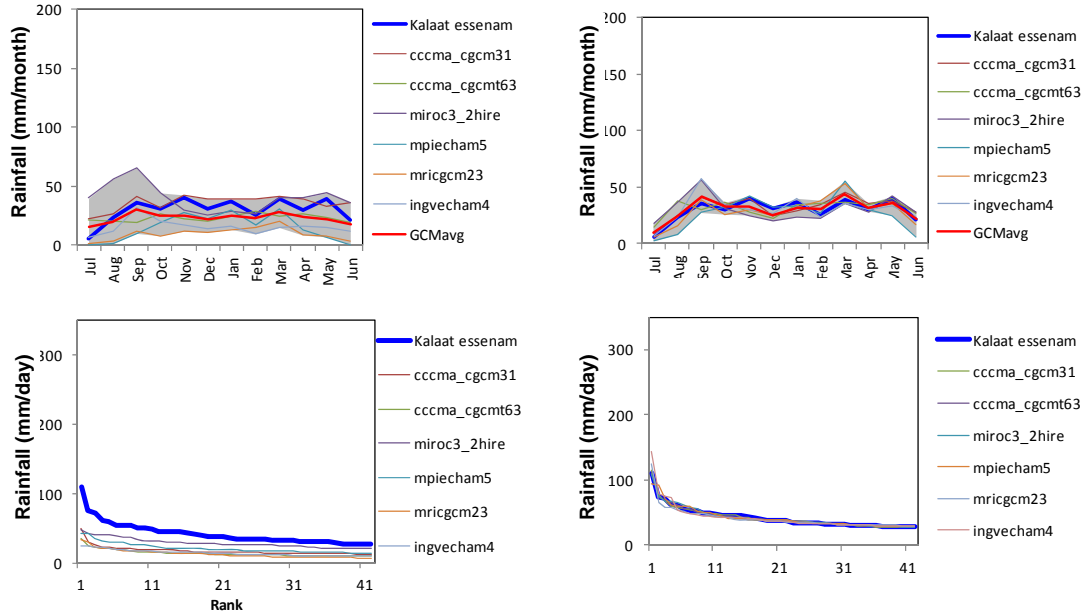


Figure II-(2)-8 The monthly average rainfalls and the extremely heavy top seventy daily rainfalls before (left) and after (right) the bias-corrections at KalaatEssenam

With regard to the extremely heavy rainfall, the bias corrected model outputs just follow the return period – rainfall intensity relationships derived from the rain gauge data as shown in **Figure II-(2)-9**.

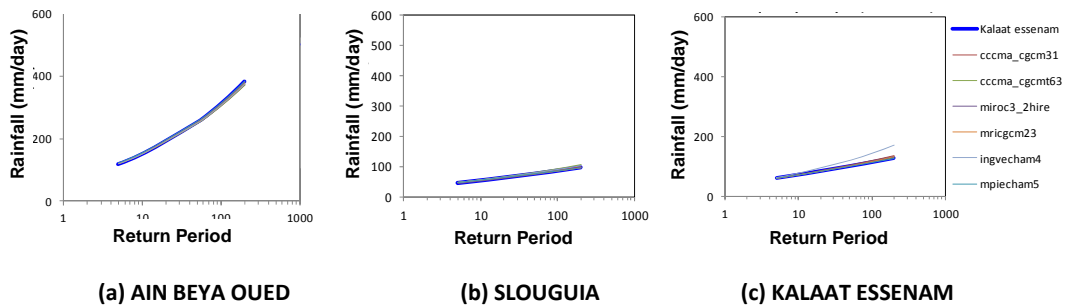


Figure II-(2)-9 The comparison of the bias corrected extreme heavy rainfall and derived from the rain gauge data

Figure II-(2)-10a and 10b show the spatial distributions of the monthly average rainfall in January before and after the bias correction of the outputs of the six GCMs, Cccmacgcm31, Cccmacgcm63, Miroc32_hires, Mpiecham5, Mricgcm23, ingv_echam4, in comparison with the rainfall map derived from the rain gauge station data. The bias of each model was corrected very successfully.

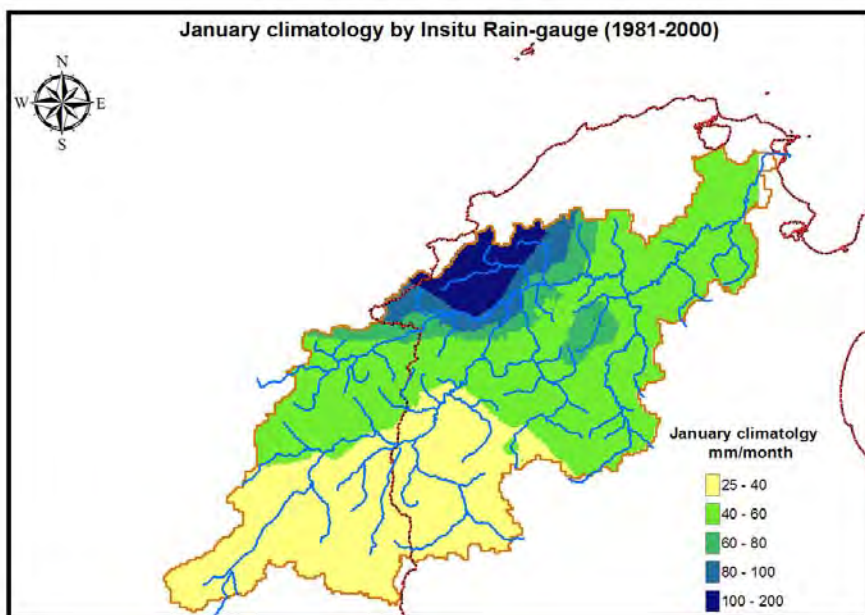


Figure II-(2)-10a The spatial distributions of the monthly average rainfall in January derived from the rain gauge station data(1981-2000)

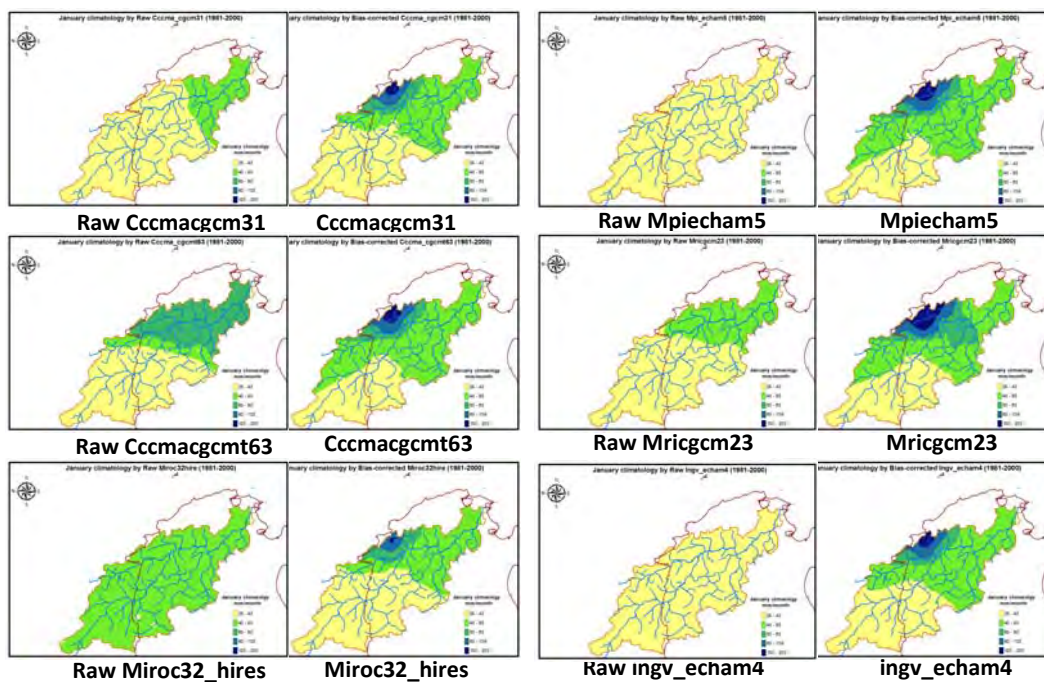


Figure II-(2)-10b The spatial distributions of the monthly average rainfall in January before (Left) and after (Right) bias correction of selected model output (1981-2000)

4. Assessment of Changes in Rainfall

All the selected models show clear dry trends with regard to the annual rainfall, the number of rain days, the seasonal rainfall, the total number of no rain days, and the annual maximum continuous dry spell at the three stations, as shown in **Figure II-(2)-11, 12, 13, 14 and 15,** respectively, without any exceptions.

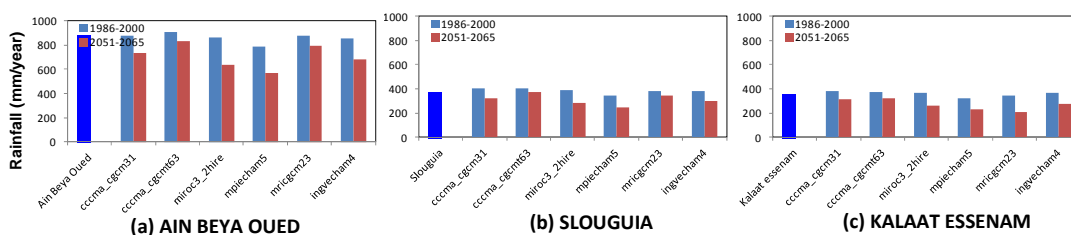


Figure II-(2)-11 Annual average rainfall at Past(Blue) and Future(Red)

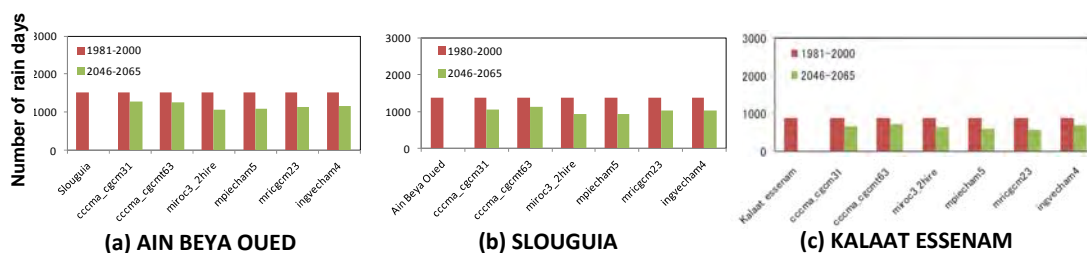


Figure II-(2)-12 The number of rain days at Past (Red) and Future (Yellow green)

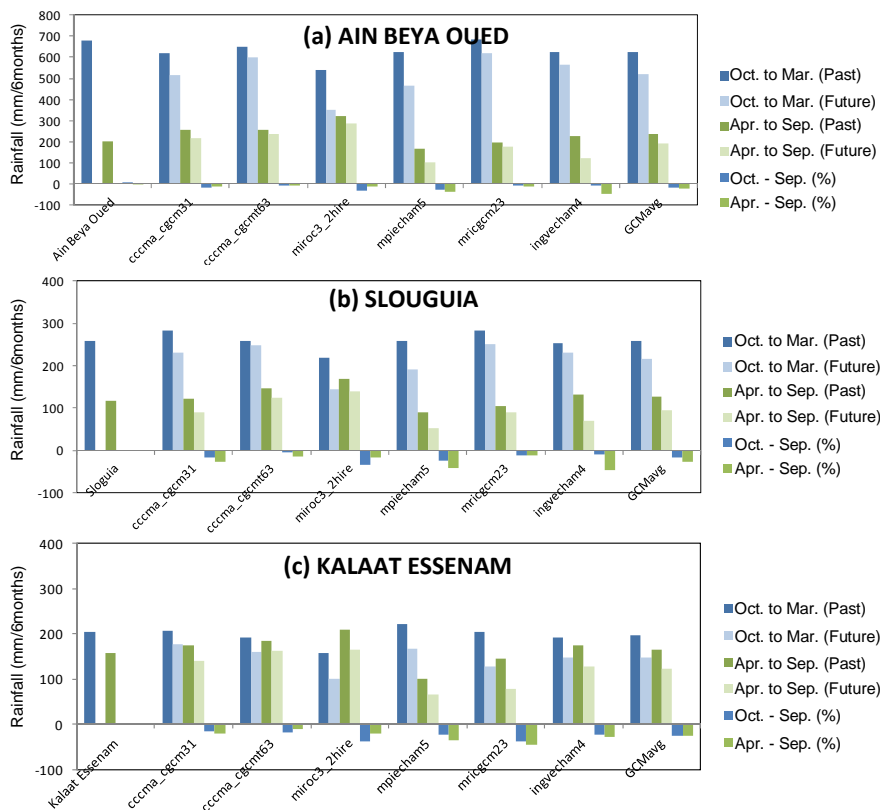


Figure II-(2)-13 The seasonal change of rainfall

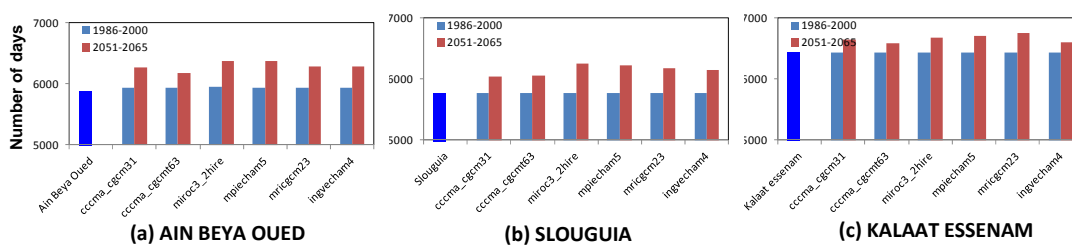


Figure II-(2)-14 The number of no rain days at Past (Blue) and Future (Red)

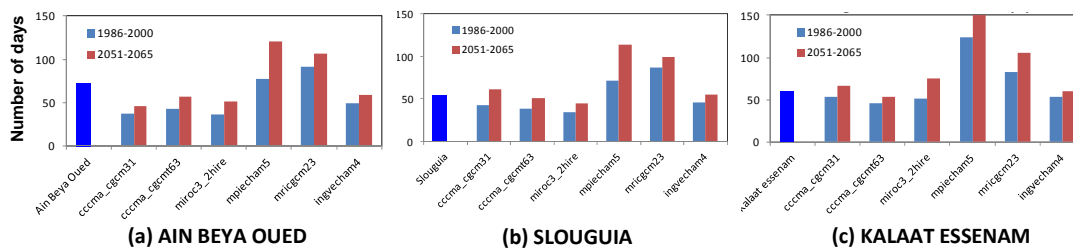


Figure II-(2)-15 The continuous dry spell at Past (Blue) and Future (Red)

Figure II-(2)-16 shows the changes of the spatial distributions of seasonal rainfall in the wet (left) and dry (right) seasons. The seasonal rainfall will decrease in the whole basin both in the wet and dry seasons. The larger decrease will appear in the upper basin during the dry season.

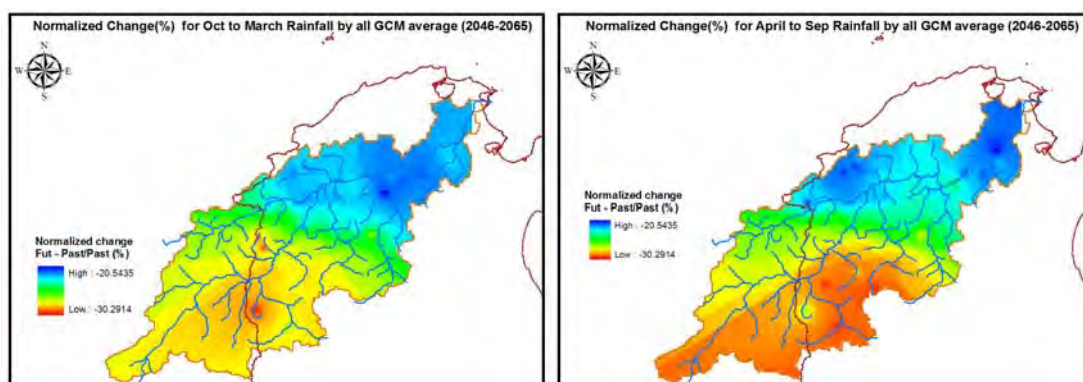


Figure II-(2)-16 The changes of the spatial distributions of seasonal rainfall in the wet (left) and dry (right) seasons

On the other hand, the changes in the extremely heavy rainfall are uncertain. **Figure II-(2)-17** shows the model-derived relationships between return period and heavy rainfall intensity in future, compared with the current one (blue thick line) derived from the in-situ data. The trend of heavy rainfall events depends on the models at Ain Beya Oued and Slougua, while almost all models show a decrease trend at Kalaat Essenam which is the driest region.

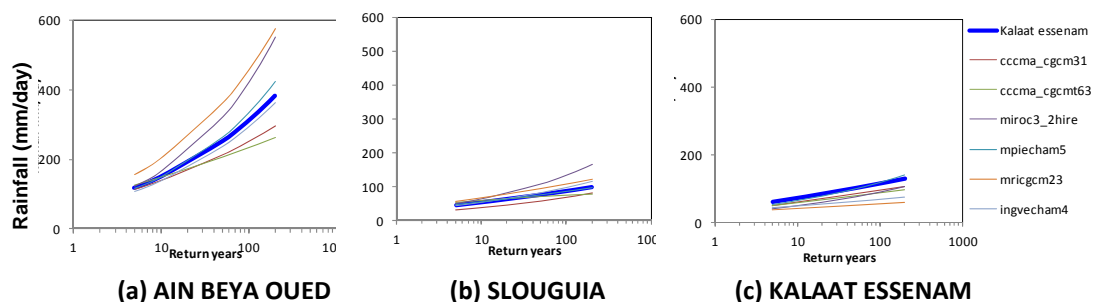


Figure II-(2)-17 The model-derived relationships between return period and heavy rainfall intensity in future and current one (blue thick line)

The averaged change of the heavy rainfall frequency will increase in the middle of the basin while decrease in the upstream as shown in **Figure II-(2)-18**. However, the differentials by each model is considerably wide.

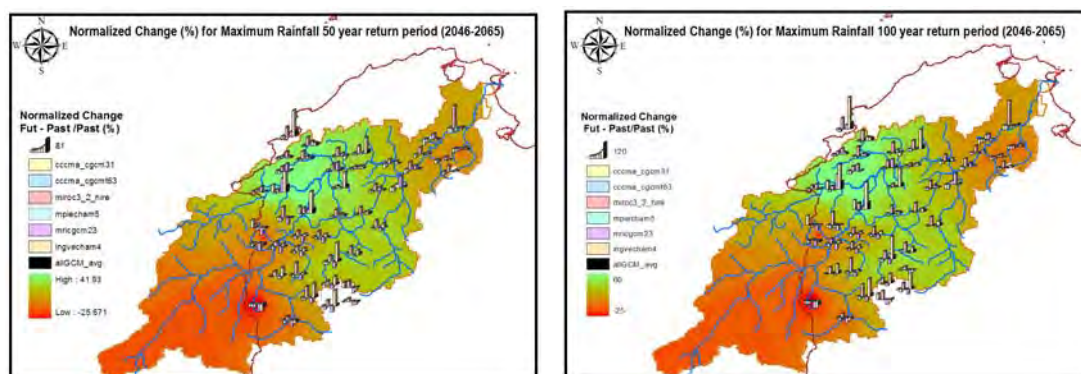


Figure II-(2)-18 The normalized change(%) of 50 year return period (left) and 100 year return period (right)

5. Assessment of Changes in the Design Floods

As discussed in the section **II-(1)-1**, 4 day rainfall is used as the design rainfall in this river basin. Firstly, the ratio of the future daily rainfall to the current one was obtained for each GCM, corresponding to each return period as shown in **Table II-(2)-4**.

Table II-(2)-4 The ratio of the current and future daily rainfall corresponding to each return period

Return years	obs [mm/d]	cccma_cgcm31	cccma_cgcm63	miroc3_2hire	mpiecham5	mricgcm23	ingvecham4
2.00	90.24	0.91	1.03	0.86	0.91	0.93	0.92
5.00	119.31	0.91	0.97	0.95	0.94	0.95	0.96
10.00	150.93	0.91	0.93	1.00	0.96	0.96	0.99
50.00	252.05	0.91	0.84	1.18	1.01	0.99	1.07
80.00	290.97	0.91	0.81	1.24	1.03	1.01	1.11
100.00	311.26	0.91	0.80	1.28	1.04	1.01	1.12
150.00	351.44	0.92	0.78	1.34	1.07	1.03	1.15
200.00	382.76	0.92	0.77	1.39	1.08	1.04	1.18

Secondly, the ratio was applied to the each design rainfall and the future 4 day rainfall for each GCM corresponding to each return period as shown in **Table II-(2)-5**.

Table II-(2)-5 The ratio applied to the each design rainfall and the future 4 day rainfall for each GCM corresponding to each return period

Return years	past	future					
		cccma_cgcm31	cccma_cgcm63	miroc3_2hire	mpiecham5	mricgcm23	ingvecham4
2	53.9	49.3	55.5	46.6	48.9	50.2	49.5
5	74.3	68.0	71.9	70.3	69.9	70.7	71.6
10	89.3	81.4	82.8	89.4	85.3	85.6	88.4
50	126.8	115.5	106.3	149.2	128.2	125.7	136.3
100	144.5	126.7	112.9	172.3	143.3	139.5	153.5

Instead of the design rainfalls obtained in the section **II-(1)-1**, the rainfall value corresponding to each return period in the **Table II-(2)-5** is input into the WEB-DHM after conversion by using the same temporal and spatial pattern in the section **II-(1)-1**. As shown in **Figure II-(2)-19**, the uncertainty of flood projection by GCMs is very large in case of large floods with the return period larger than 50 years due to their large run-off ratio, while it is small in the case of small or middle-sized floods with the return period shorter than 10 years due to the small ratio. The difference of the effects of climate change on flood projection uncertainty is explained as one of the characteristics of semi-arid river basins such as Mejerda River.

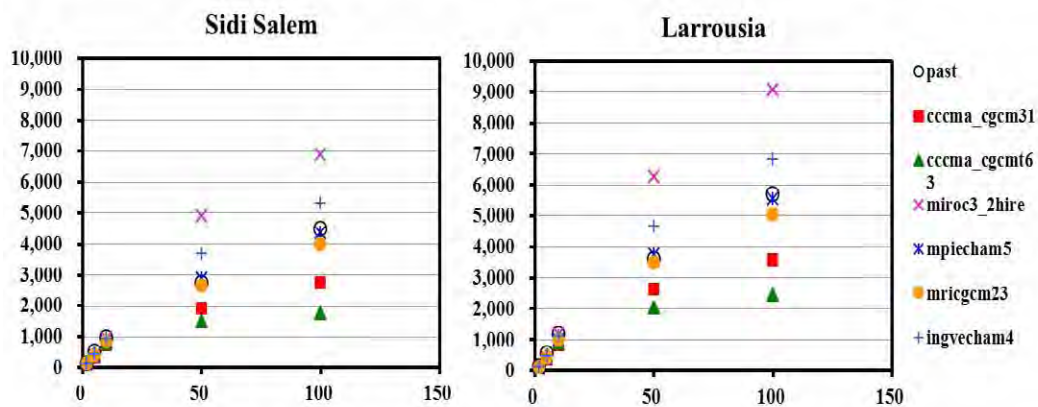


Figure II-(2)-19 The relationship between design flood and return period at Sidi Salem (left) and Larrousia (right).

(3) Optimizing Dam Operation

To balance various demands from different stakeholders, a systematic approach is needed for the real-time optimization of dam release in a river basin. Optimization techniques together with simulation models are often used to deal with reservoir operation problems, since the use of optimization models for identifying policies for the real-time dam releases can be quite beneficial. Regarding river basins with different sizes, the lead times (corresponding to the travel time to a downstream flooding location) necessary for an effective dam operation (for disaster mitigation) can be quite different, closely linked with the selection of precipitation inputs for the simulation model. A large river basin has usually a longer flow distance from upstream to downstream, and this makes it possible to operate a downstream dam in a real-time manner, with the observed precipitation even at the upstream.

This section introduces an integrated simulation and optimization system (ISOS, Wang et al., 2013), which comprises a distributed biosphere hydrological model and a global optimization system, and employs the rolling horizon approach to determine near-real time dam releases. **Figure II-(3)-1** shows the flowchart for achieving an optimal rule for dam operation.

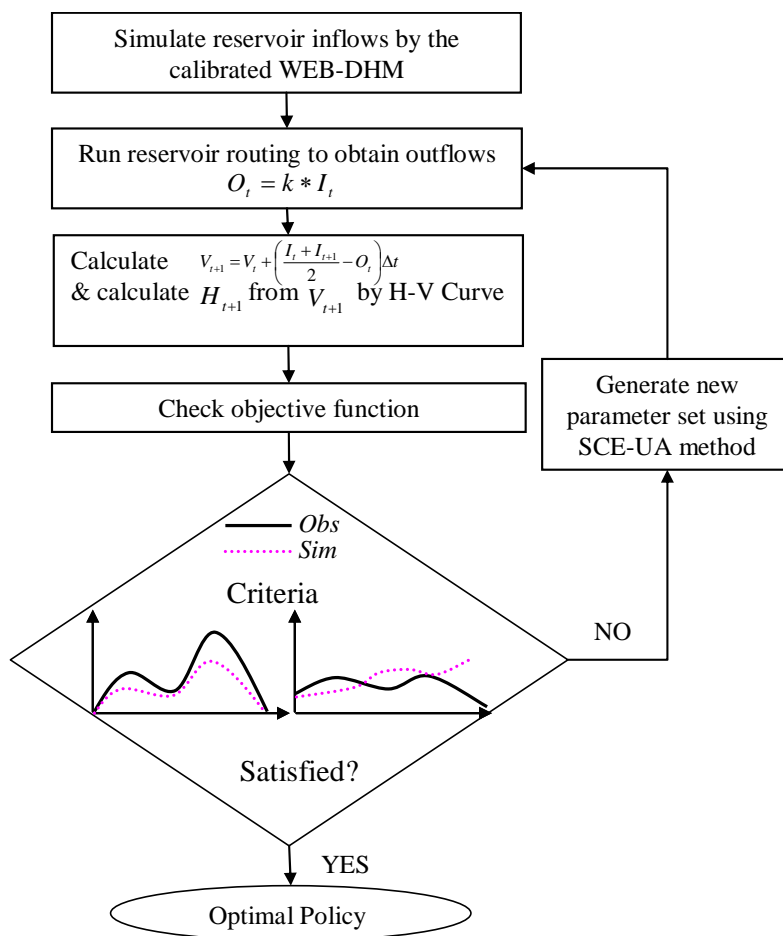


Figure II-(3)-1 The flowchart to calculate optimized dam operation rule

1. Hydrological Model

The ISOS uses the WEB-DHM developed in the section II-(1)-1 as its key simulator. To introduce this model to the functions of the Sidi Salem Dam, a simple storage function for reservoir routing in a river network was added to the WEB-DHM (Yang et al., 2007). According to the third box of **Figure II-(3)-1**, the storage in the next time step can be approximately derived and estimated by the reservoir water level for the current time step with using reservoir characteristics (H-V curve).

2. Global Optimization System

A global optimization scheme, the Shuffled Complex Evolution (SCE, Duan et al., 1992, 1993, 1994) was used as the optimizer in the ISOS. The SCE method comprises a synthesis of the following four concepts:

- 1) combination of deterministic and probabilistic approaches;
- 2) systematic evolution of a complex of points spanning in the parameter space, in the direction of global improvement;
- 3) competitive evolution; and
- 4) complex shuffling.

The SCE scheme is expected to obtain the parameter set that can produce a good approximation to the global optimum of the objective function which includes both flood control and water use.

3. Rolling Horizon Approach

The reservoir operation employs a rolling horizon approach. As shown in **Figure II-(3)-2**, it generally comprises procedures as:

- 1) making the release decision in forecast horizon with a limited forecast;
- 2) implementing the current release decision in decision horizon; and
- 3) moving to the next period and repeat (1) and (2) with updated inflow forecast and reservoir storage until the end of operation horizon.

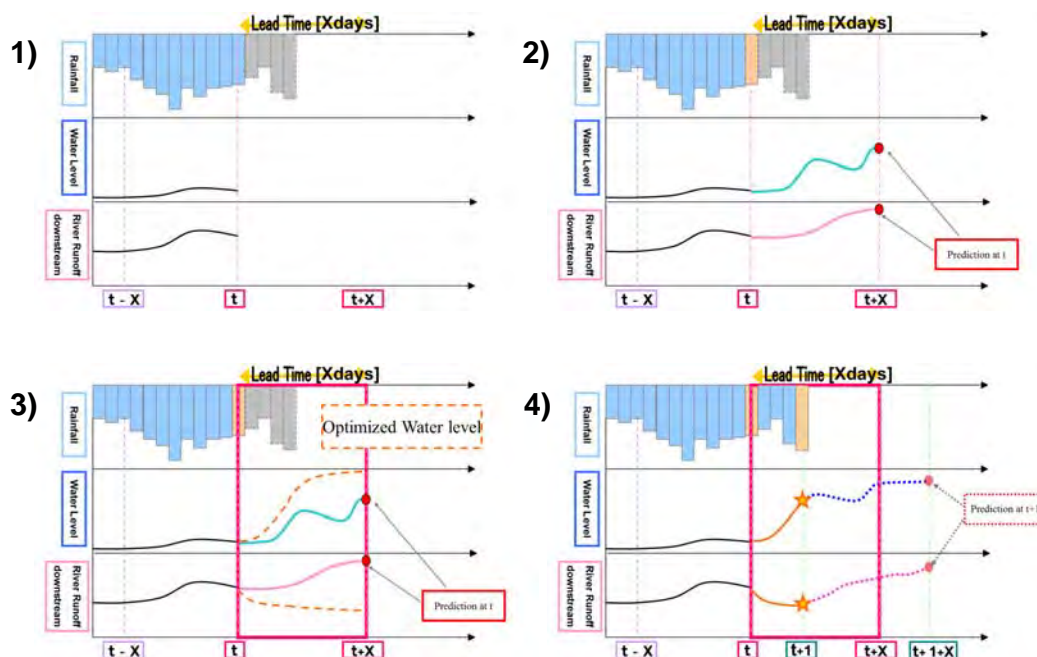


Figure II-(3)-2 Rolling horizon approach

4. ISOS Procedure

The ISOS procedure can be described as:

- 1) Distributed soil hydraulic parameters of WEB-DHM are calibrated for each dam's inflow, and the calibrated model is then used to predict dam inflow during reservoir optimization.
- 2) For each optimization run, the optimal reservoir release is calculated by using the new optimal parameter generated by SCE (considering both the reservoir water level and the flood at a downstream point) towards the global optimum of the objective function.
- 3) After each optimization run, the integrated optimal operational rule is determined.
- 4) Steps (2) and (3) are repeated until the predefined criteria (related to flood reduction and water use) are satisfied.

5. ISOS Demonstration

The ISOS was applied to the Mejerda River Basin. The ratio of the dam release to the inflow into the reservoir is optimized in the case of the first peak of the flood in January 2003 by using SCE under the following two conditions:

- the water level (H) of the Sidi Salem Dam gets close to EL.115m just after the flood but not higher than EL. 115m.
- the dam release (Q_{out}) is less than $800 m^3 / s$

The cost function is expressed by using the same weight of flood control and water use as follows:

$$0.5 \times \sqrt{\frac{\sum_{i=1}^N (Q_{out} - 800)^2}{N}} + 0.5 \times \sqrt{\frac{\sum_{i=1}^N (H - 115)^2}{N}} \quad (11)$$

As shown by the red lines in **Figure II-(3)-3**, three day flood prediction issued every day is used for optimization of flood control and water use. Considering the flood travel time, the optimized operation of the first day of the three days was used for the decision as shown by blue circles on **Figure II-(3)-3** for dam release and red circles on **Figure II-(3)-4** for reservoir water level.

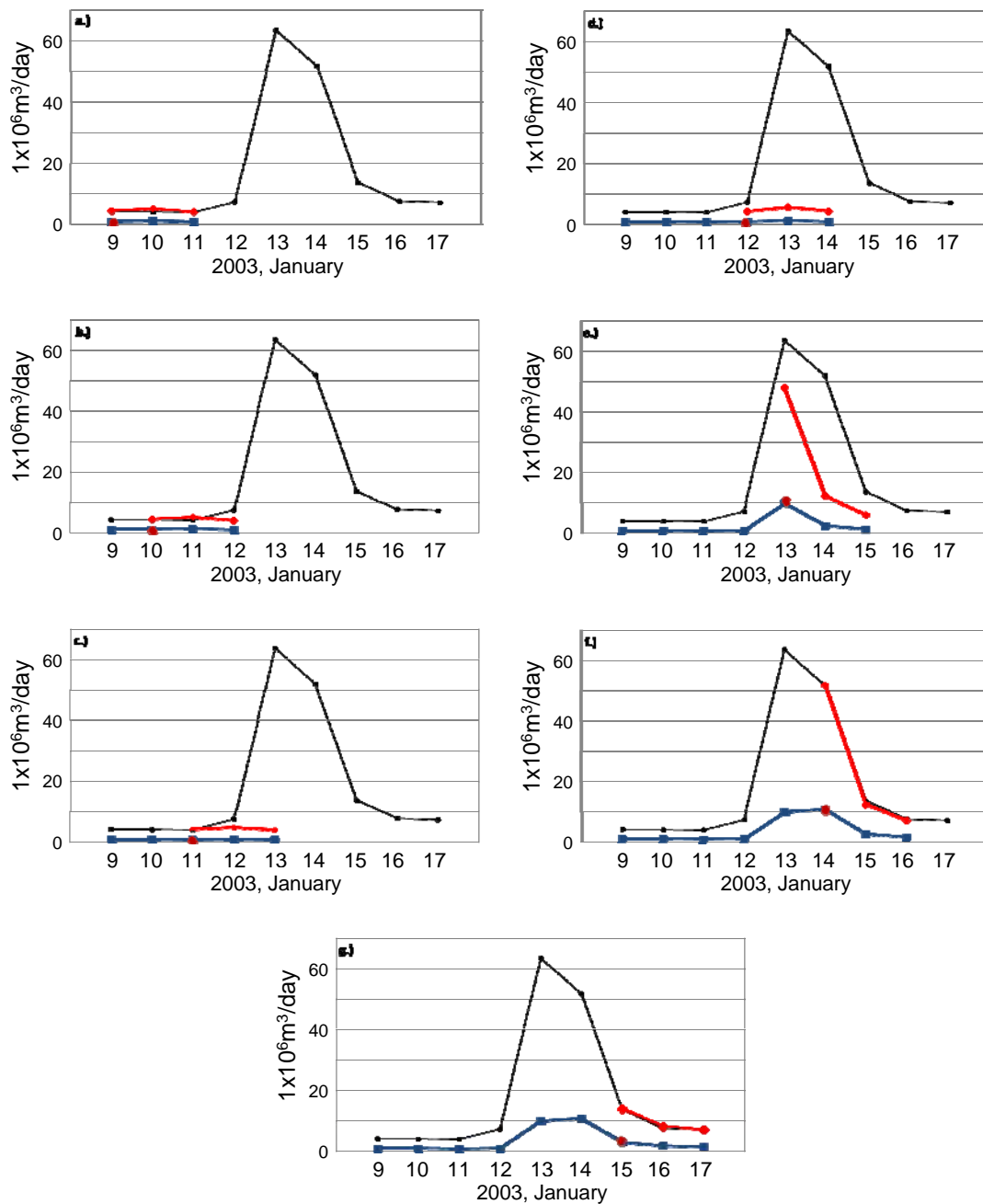


Figure II-(3)-3 Dam inflow(Obs. Black, Est. Red) and outflow

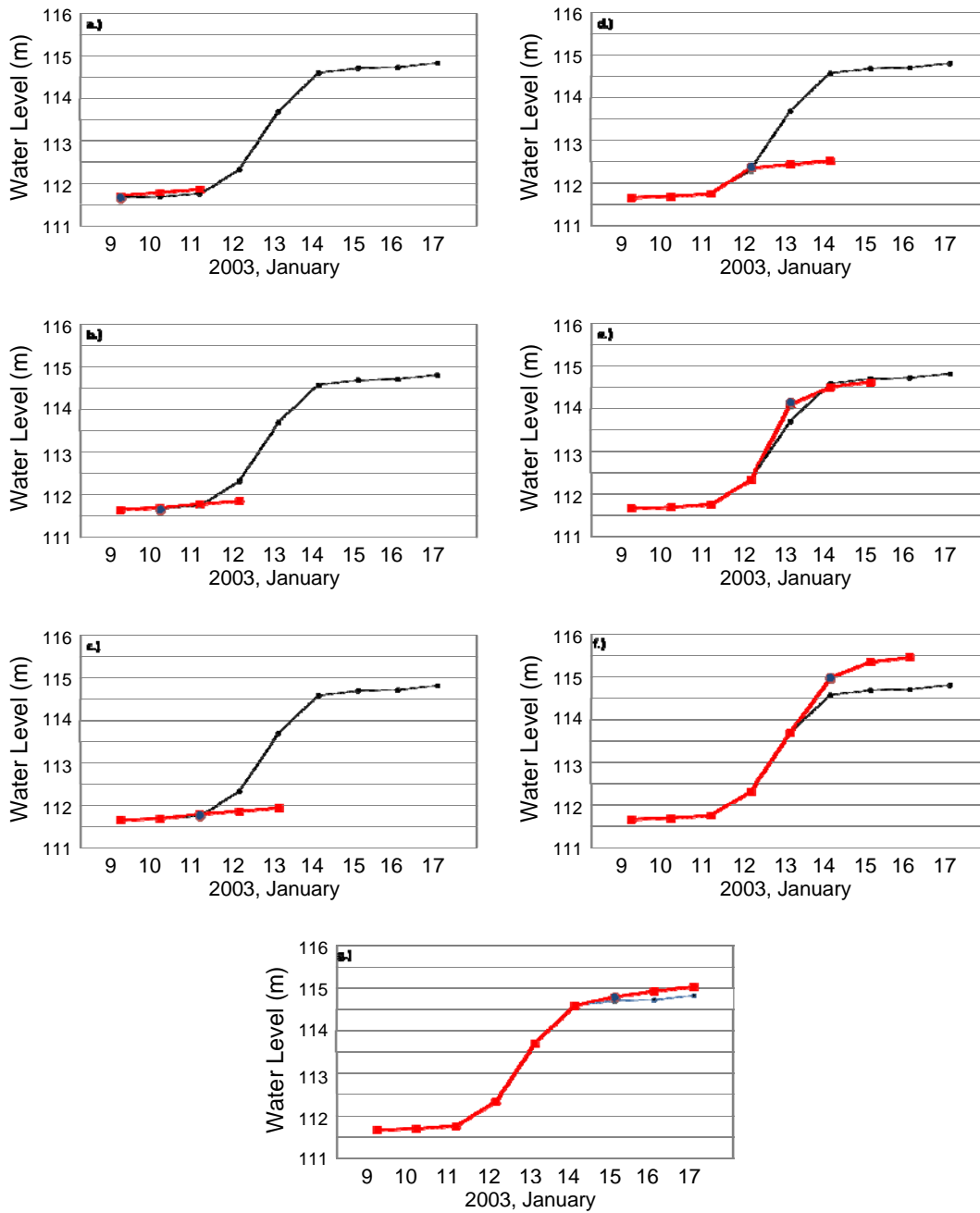


Figure II-(3)-4 Dam water level (Obs. Black, Est. Red)

Figure II-(3)-5 shows the result of the optimization. The predicted inflow colored by red is close to the observed one by orange. The dam actually released a lot of water at the end of the flood as shown by the light blue line on Figure II-(3)-5, while ISOS could reduce the dam release, store the water and make the reservoir water level finally to reach the maximum value, 115m, successfully at the end of the flood.

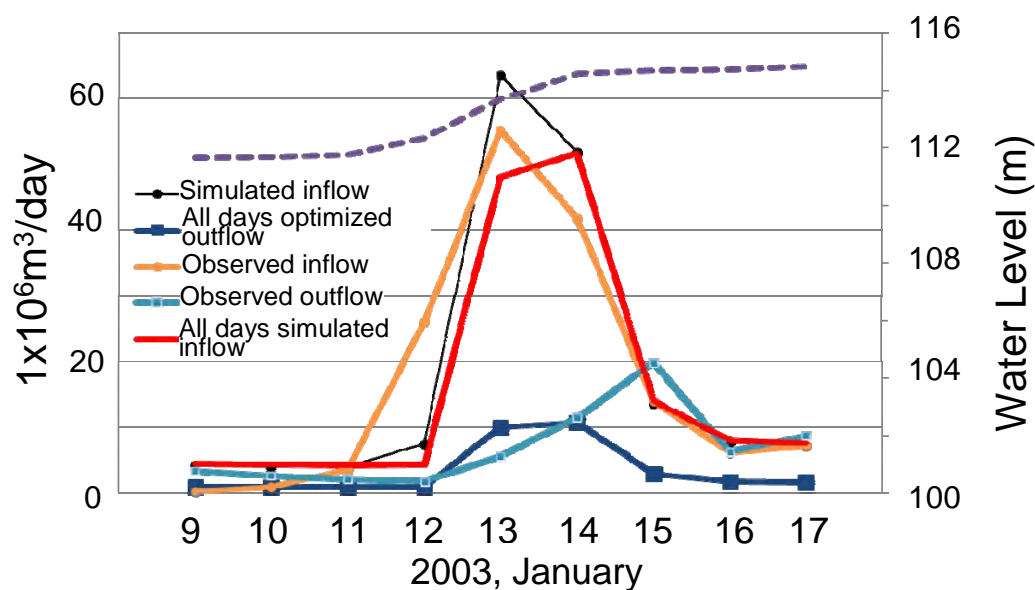


Figure II-(3)-5 Optimized dam operation result

III. Conclusions and Recommendations

This study presents three results.

- (1) Design rainfall, design flood discharge before regulation and design flood discharge after regulation were estimated by using the statistical analysis of the observed rainfall data and a distributed hydrological model (WEB-DHM) which can simulate soil moisture and river runoff without any tuning for a long term.
- (2) Climate change impact assessment was implemented by using the GCM outputs after bias correction and down-scaling coupled with the in-situ data and the global scale data products. The results of the assessment shows the very clear dry tendency in future and the large uncertainty in the flood projection. Especially, the large flood projection has large uncertainty.
- (3) A case study shows that the optimization of dam operation works effectively both for flood control and for water use.

We suggest the following proposals and recommendations for the water resources management in the Mejerda River Basin based on our above conclusions.

- (1) To design and establish long-term and more advanced observing systems and a real time data utilization system in an early stage.
- (2) To improve understanding of hydrological characteristics of Mejerda River under the large climate gradient from the Mediterranean Sea to the inland area and to prepare for a long-term water resources management and a short-term adaptation measures against, especially targeting large flood even under a clear drought-prone trend. .
- (3) To build capacity for promoting observation system design and management, effective use of climate projection model outputs, development and application of distributed hydrological models for long-term simulation of river run-off from low flow to high flow and soil moisture, and optimization of dam operation.

References

- 1) Duan Q, Sorooshian S, Gupta VK.: Effective and efficient global optimization for conceptual rainfall-runoff models. *Water Resources Research* 28(4): 1015-1031, 1992.
- 2) Duan Q, Sorooshian S, Gupta VK. : Shuffled complex evolution approach for effective and efficient global minimization. *Journal of Optimization Theory and Applications* 76(3): 501-521, 1993.
- 3) Duan Q, Sorooshian S, Gupta VK.: Optimal use of the SCE-UA global optimization method for calibrating watershed models. *Journal of Hydrology* 158: 265-284, 1994.
- 4) Feddersen H., and U. Andersen: A method for statistical downscaling of seasonal ensemble predictions. *Tellus*, 57A, 398-408, 2005.
- 5) Ines A. V. M., and J. W. Hansen: Bias correction of daily GCM rainfall for crop simulation studies, *Agricultural and Forest Meteorology*, 138, 44-53, 2006.
- 6) IPCC: IPCC Special Report on Emissions Scenarios, Chapter 4, IPCC WG III, COP 6, Hague, 2000.
- 7) NYUNT, C.T., T.KOIKE, P.A.J. SANCHEZ, A. YAMAMOTO, T. NEMOTO and M. KITSUREGAWA: Bias Correction Method for Climate Change Impact Assessments in the Philipines, *Journal of Japan Society of Civil Engineers, Ser. B1 (Hydraulic Engineering)*, Vol.69, No.4. I_19-I_24, 2013
- 8) Sellers, P. J., D. A. Randall, G. J. Collatz, J. A. Berry, C. B. Field, D. A. Dazlich, C. Zhang, G. D. Collelo, and L. Bounoua: A revised land surface parameterization (SiB2) for atmospheric GCMs, Part I: Model formulation, *J. Clim.*, 9, 676-705, doi:10.1175/1520-0442(1996)009<0676:ARLSPF>2.0.CO;2.
- 9) Sharma D, Das Gupta A, Babel MS: Spatial disaggregation of bias-corrected GCM precipitation for improved hydrologic simulation: Ping river basin, Thailand. *Hydrol Earth Sys Sci* 11(4):1373–1390, 2007.
- 10) Yang, D., S. Herath, and K. Musiak (2000), Comparison of different distributed hydrological models for characterization of catchment spatial variability, *Hydrol. Processes*, 14, 403–416, doi:10.1002/(SICI)1099-1085(20000228)14:3<403::AID-HYP945>3.0.CO;2-3.
- 11) Yang, K., T. Watanabe, T. Koike et al.: Autocalibration System Developed to Assimilate AMSR-E Data into a Land Surface Model for Estimating Soil Moisture and the Surface Energy Budget, *Journal of the Meteorological Society of Japan*, Vol.85A, pp 229-242, 2007.
- 12) Wang, L., T. Koike, K. Yang, T. J. Jackson, R. Bindlish, and D. Yang, Development of a distributed biosphere hydrological model and its evaluation with the Southern Great Plains Experiments (SGP97 and SGP99), *J. Geophys. Res.*, 114, D08107, doi:10.1029/2008JD010800, 2009.
- 13) Wang L., T. Koike, M. Ikeda, C. T. Nyunt, D. N. Tinh, O. Saavedra, T. V. Sap, L. C. Nguyen, K. Tamagawa, T. Ohta: Optimizing multi-dam releases in large river basins by combining distributed hydrological inflow predictions with rolling horizon decision making, *Journal of Water Resources Planning and Management*, submitted, 2013.